THESIS

A TRANSPIRATION-DRIVEN MASS-BALANCE FRAMEWORK FOR QUANTITATIVE ANALYSIS OF NUTRIENT UPTAKE IN *CANNABIS SATIVA* L.

Submitted by

Kit Powell

Department of Horticulture and Landscape Architecture

In partial fulfillment of the requirements

For the Degree of Master of Science

Colorado State University

Fort Collins, Colorado

Summer 2026

Master's Committee:

Advisor: Bill Bauerle

Joshua Craver
Jose Chavez

ABSTRACT

A TRANSPIRATION-DRIVEN MASS-BALANCE FRAMEWORK FOR QUANTITATIVE ANALYSIS OF NUTRIENT UPTAKE IN *CANNABIS SATIVA* L.

Nutrient management that replenishes plant uptake from solution begins with a knowledge of the amount of nutrients roots extracted from the nutrient solution and how that quantity changes over the plant's lifecycle. This thesis tests a physiology-informed mass-balance framework for estimating *Cannabis sativa* L. nutrient requirements by coupling whole-plant nutrient uptake with water removed by transpiration. Changes in the amount of nutrients taken up with water are determined by multiplying the concentration of nutrients in organ tissue, by fluctuations in plant water use efficiency (WUE). WUE and variations in the nutrient requirement, therefore, adjust the nutrient replenishment calculated concentrations in relation to the environment and plant genetics. Electrical Conductivity (EC) reports ionic strength, not ion identity or balance, so equal EC values can mask very different nutrient profiles. Similarly, fixed nutrient input setpoints can obscure ion selective uptake and the accumulation of unused ions in solution can result. Furthermore, determining nutrient replenishment solutions using leaf-only nutrient concentrations bias element input prescriptions because organs differ in element composition and storage in addition to uptake amounts that change with phenology. We found that flowers often accumulate potassium [K] and phosphorus [P] in excess, while stems and roots contain proportionally more calcium [Ca] and magnesium [Mg]. Element mobility and transport pathways also vary with sink strength, which was an additional impetus for us to investigate organ biomass-weighted nutrient uptake predictions validated against leachate and tissue concentrations.

We implemented this framework for two cultivars, CJ2 and First Light, in containerized substrate culture across the *Cannabis sativa* L. vegetative and reproductive phase, to estimate nutrient uptake from plant tissue concentrations using three physiologically driven observations: continuous gravimetric measurement of transpiration, pour-through leachate analysis of residual solution element composition, and organ-level analysis of tissue nutrient concentrations. In the vegetative phase, nutrient uptake tracked canopy growth and water use. Nitrogen [N] and potassium [K] uptake increased with leaf area, while calcium [Ca] and magnesium [Mg] uptake escalated as vascular transport matured and sinks shifted toward structural growth. Organ biomass-weighted mean element input calculations aligned more closely with solution nutrient drawdown than single organ input calculations during the vegetative stage, which prompted us to investigate nutrient uptake during the flowering phase. Because the biomass-weighted mean among organs outperformed single-organ proxies in vegetative plants, we next tested whether that advantage persisted through the reproductive phase, when sinks and transport pathways shift toward regenerative growth. In the regenerative phase, N leaf tissue element concentration calculations overpredicted uptake by 34.3% in CJ2 and 25.6% in First Light, roots underpredicted by 19.4% and 5.9%, and stem nutrient input estimates were lower than uptake by 36.3% and 37.3%. For P, root tissue nutrient concentrations in conjunction with WUE were closest to nutrient uptake from solution, slightly higher in CJ2 (+7.5%) and lower than observed uptake in First Light (−20.3%), while stem concentrations underpredicted uptake by about 60% in both cultivars. For Mg, the organ biomass-weighted mean input estimate was between other organ tissue uptake calculations, resulting in 38.3% and 49.8% less than predicted uptake compared to actual observed uptake from solution. For micronutrients, agreement was element specific once tissue values were adjusted per liter of transpired water. Several micronutrient calculations of input concentration were a near match with that of uptake, whereas others showed modest underprediction. Excluding flowers from the organ biomass-weighted mean during periods of

inflorescence luxury accumulation improved whole-plant nutrient uptake prediction accuracy.

Our results show that nutrient uptake scales with whole-plant WUE. Periodic validation against leachate and tissue nutrient profiles can adjust for phenological shifts in nutrient uptake and partitioning to improve nutrient input predictions. Plants take up only a fraction of the nutrients supplied. By quantifying baseline uptake in *Cannabis sativa* L. and coupling it to water use and whole-plant nutrient partitioning, the result of this research supports the adoption of a physiologically based mass-balance framework for estimating nutrient prescriptions. In addition, we found that calculations can reproduce whole-plant nutrient requirements in different cultivars and throughout distinctly different plant growth stages. The result is greater efficiency of resources, less waste, and a nutrient input supply that mirrors uptake requirements in semi-closed substrate systems.

ACKNOWLEDGEMENTS

The Colorado Nursery and Greenhouse Association
The Cannabis Research Institute in Pueblo
Colorado State University Experiment Station
Bill Bauerle
Joshua Craver
Jose Chavez
Ian Aksland
Hunter Konchan
Mike Hazlett

TABLE OF CONTENTS

CHAPTER 1: LITERATURE REVIEW

1.1 Introduction

Nutrient management is central to sustainable plant production and environmental stewardship. Although substantial progress has been made in refining nutrient delivery in controlled-environment agriculture hydroponic systems, most studies to date have focused on identifying upper thresholds of nutrient supply beyond which additional inputs no longer enhance growth or quality (Hershkowitz et al., 2025; Saloner & Bernstein, 2022; Shiponi & Bernstein, 2021; Westmoreland & Bugbee, 2022). Furthermore, studies demonstrate that luxury uptake is common in high-value crops such as *Cannabis sativa* L. (*C. sativa*), particularly during reproductive development, and that excessive nutrient supply can reduce resource-use efficiency (Hershkowitz et al., 2025; Westmoreland & Bugbee, 2022). However, the current literature largely overlooks an equally critical question: what quantity of nutrients do plants uptake from solution under non-limiting conditions? Defining base uptake is fundamental to establishing physiologically optimal nutrient input concentrations for hydroponic nutrient replenishment solutions. This need is particularly important for *C. sativa*, whose propensity for inflorescence luxury nutrient uptake makes it an ideal model to differentiate physiological demand from unnecessary uptake. Despite *C. sativa's* economic significance, there are a lack of studies that quantify baseline nutrient uptake throughout its life cycle.

In contrast to hydroponic systems where roots are continuously immersed in solution, substrate systems provide nutrients episodically and maintain only intermittent root–solution contact, complicating the quantification of temporal uptake dynamics and solution depletion. This knowledge gap is acute in substrate systems because most hydroponic nutrient uptake research to date has been conducted in recirculating deep water culture systems, where nutrient solutions remain in continuous contact with the root system

and changes in solution concentration can be directly attributed to plant uptake (Bugbee, 2004; Hershkowitz et al., 2025; Langenfeld et al., 2022). While these studies have yielded valuable insights into nutrient uptake, they may not be directly applicable to discrete-solution substrate environments, where nutrient availability and root–solution contact vary over time. For example, Shiponi and Bernstein (2021) reported optimal phosphorus levels at ~30 ppm in substrate-grown *C. sativa*, whereas Westmoreland and Bugbee (2022) found no improvement in yield or quality when phosphorus supply was elevated above 15 ppm in a recirculating deep-water culture system (Shiponi & Bernstein, 2021; Westmoreland & Bugbee, 2022). More recently, Hershkowitz et al. (2025) and Westmoreland and Bugbee (2022) confirmed that substantial increases in phosphorus concentration, up to 90 ppm, did not enhance yield or cannabinoid production (Hershkowitz et al., 2025; Westmoreland & Bugbee, 2022). Because substrate fertigation events create transient nutrient concentrations and fluctuating root–solution contact, quantifying uptake under these common plant production conditions is essential for developing nutrient input prescriptions that fulfill physiological requirements, maximize plant growth, and optimize resource use efficiency.

Consequently, a stronger empirical foundation is required to quantify the baseline amount of nutrients extracted by plants from substrate solution under conditions of adequate availability. Such information is necessary to align fertigation schedules with physiological demand for nutrients, which can directly advance sustainable cultivation practices (Langenfeld et al., 2022). This is of particular importance for *C. sativa*, a crop with a demonstrated capacity for inflorescence luxury uptake and industry-standard nutrient regimes that often exceed plant requirements (Hershkowitz et al., 2025; Westmoreland & Bugbee, 2022). Quantifying nutrient uptake under substrate conditions will therefore enable more precise supply strategies that support both optimal plant performance and resource-use efficiency.

Plants acquire essential mineral elements primarily from the rhizosphere (Cui, 2012; White & Brown, 2010). This acquisition can be rigorously quantified using the conservation-law of mass balance, which enables complete accounting of nutrient inputs and internal storage at the plant scale (Cogley, 2010; Langenfeld et al., 2022). Moreover, mass balance provides a framework to track nutrient uptake and organ-specific accumulation over time. In controlled environments, closed-loop fertigation permits steady-state nutrition where water removed by transpiration is replaced with solution containing the nutrients taken up with that water (Langenfeld & Bugbee, 2024). This links nutrient delivery to transpiration demand and improves nutrient-use efficiency (NUE). However, open-system field-scale nutrient budgets initially compared fertilizer application to crop removal and estimated losses (Parent et al., 2012). Subsequent work incorporated organ-level partitioning and remobilization (Chen et al., 2019), recognizing that mobile nutrients (e.g., nitrogen and potassium) are redistributed, whereas immobile nutrients (e.g., calcium and boron) remain localized (Massuela et al., 2023). These nutrient budget accounting differences provided us with an impetus to investigate organ biomass-weighted calculations for nutrient input concentrations rather than rely on leaf-only elemental composition.

A key advance from Langenfeld et al. (2022) was to compute irrigation solution element concentrations as leaf target tissue concentrations × whole-plant WUE (yielding nutrient input concentration; mg L^{-1}). Elevated atmospheric CO_2, however, increases WUE by reducing stomatal conductance, thereby decoupling nutrient supply from water flux and requiring upward adjustment of nutrient concentrations to maintain steady-state conditions (Langenfeld et al., 2022). Therefore, WUE, which typically ranges from ~3 g L^{-1} at ~400 ppm CO_2 and ~40% RH to ~6 g L^{-1} at ~1200 ppm CO_2 and ~70% RH, can change by a factor of two across common controlled environment agriculture conditions (Langenfeld et al., 2022). WUE, therefore, functions to adjust the nutrient replenishment concentrations in relation to changes in the environment and plant genetics. When non-leaf organs constitute a substantial fraction of biomass and exhibit element concentrations distinct from leaves,

reliance on leaf tissue values alone can overestimate demand (Chen et al., 2019). We therefore advance an organ-explicit biomass-weighted accounting framework that links nutrient input calculations to developmental stage uptake and transpiration-driven water use. This approach reconciles solution nutrient depletion with whole-plant nutrient uptake, which we independently evaluate using pour-through leachate analysis (Altland, 2021).

1.2 Nutrient Cycling and Uptake Dynamics

Uptake rates differ by element: active (nitrogen, phosphorus, potassium, manganese), intermediate (magnesium, sulfur, iron, copper, zinc, molybdenum, nickel, chloride), and passive (calcium and boron), which alters residual solution composition through time and can lead to imbalances in recirculating nutrient solutions (Bevan et al., 2021; Langenfeld et al., 2022). Because actively absorbed ions decline rapidly, electrical conductivity (EC) frequently decreases during exponential growth. In addition, the differential rate of nutrient uptake results in three elements (calcium, magnesium, and sulfate) as the primary remaining contributors to EC. This can result in nontrivial cation/anion nutrient imbalance within the solution if EC, which does not describe the solution composition, is relied upon to quantify solution nutrient concentration. Under such circumstances, cation–anion imbalances can impair uptake of specific nutrients and increase the risk of phytotoxicity. These dynamics are particularly relevant in *C. sativa*, where pronounced luxury uptake is prevalent in the flowers (Hershkowitz et al., 2025; Massuela et al., 2023; Shiponi & Bernstein, 2021; Westmoreland & Bugbee, 2022).

1.3 Challenges in Model Validation and Heterogeneity

A growing body of literature has demonstrated that nutrient demand in plants is temporally dynamic and closely coordinated with phenological development, such that uptake rates reflect stage-specific shifts in physiological sinks. In cereals such as rice (*Oryza sativa*), grain nutrient accumulation is rapid and element-specific during the endosperm filling phase (10–30 days after fertilization), with iron continuing to accumulate while other elements, including phosphorus, potassium, and zinc, decline in concentration due to

biomass dilution (Ram et al., 2020). In perennial systems, sequential whole-tree sampling has shown that newly formed tissues, though comprising a small fraction of total biomass, act as major nutrient sinks. These findings have led to the development of phenology-linked nutrient budget curves, particularly in high-value orchard crops such as avocado, enabling the alignment of nutrient supply with temporal demand to improve fertilization precision (Silber et al., 2018). More recent efforts have integrated mass balance principles with transpiration-driven metrics to estimate nutrient demand as a function of water use, providing a tractable and physiologically grounded framework for nutrient management (Langenfeld et al., 2022; Sperling, 2020). However, validation of time-resolved nutrient uptake models remains challenging under heterogeneous soil conditions (Griffiths & York, 2020), as genotypic differences in uptake capacity, genotype-linked variation in rhizosphere microbiome composition, and spatial heterogeneity in substrate exchange and sorption processes, further complicate nutrient-flux closure (Ahmadi et al., 2024; Ahmed et al., 2021; Barrow et al., 2024; Hinsinger, 2001; Shen et al., 2011; Shiponi & Bernstein, 2021). In addition to these external sources of variability, the lack of comprehensive data on internal nutrient recycling and remobilization limits model accuracy (Ahmed et al., 2021; Massuela et al., 2023). Temporal variability in WUE underscores the need for dynamic nutrient supply models that integrate real-time sensor feedback rather than relying on static prescription-based approaches (Langenfeld et al., 2022).

Collectively, these aspects illustrate the importance of coupling phenology-driven nutrient demand models with dynamic environmental and physiological adjustments to improve predictive accuracy and NUE across diverse cropping systems. Temporal heterogeneity in nutrient uptake is particularly evident in *C. sativa*, where reproductive sinks dominate allocation and undermine predictions derived from static organ-specific models (Hershkowitz et al., 2025; Shiponi & Bernstein, 2021). Therefore, time-resolved nutrient uptake models validated under substrate conditions are warranted.

1.4 Expanding Beyond Leaf Tissue Nutrient Concentrations

Advancing the organ biomass-weighted mass-balance concept beyond the model of total biomass × WUE × leaf tissue element concentration necessitates explicit organ-specific quantification of nutrient partitioning among roots, stems, leaves, and reproductive organs, particularly for immobile elements such as calcium and boron, whose restricted phloem mobility leads to localized accumulation in transpiring or structural tissues (e.g., young leaves, stems, and roots) (White & Broadley, 2003). Empirical studies in modern soybean cultivars reveal that nutrients such as nitrogen, phosphorus, calcium, magnesium, and boron follow distinct organ-specific partitioning patterns, with considerable variability in harvest index across elements (Bender et al., 2015). These patterns highlight the limitations of relying solely on leaf tissue concentrations to estimate whole-plant demand—particularly during flowering, when organ concentrations diverge and remobilization increases (Massuela et al., 2023). Solution drawdown measured by the validated pour-through method provides an operational check on model estimates (Altland, 2021); in cannabis, leachate chemistry is responsive to nutrient fluxes even when yield is unchanged (Westmoreland & Bugbee, 2022).

Thus, we propose an organ-weighted framework that matches solution depletion with tissue nutrient concentrations that are representative of whole-plant nutrient requirements. This is especially critical in cultivars with high stem or root biomass fractions or in those exhibiting strong reproductive sink development, where down-weighting leaf tissue concentrations yield a more accurate representation of whole-plant nutrient demand. Incorporating organ biomass-weighted element requirements into mass-balance calculations has the potential to enhance model reliability across nutrients with diverse mobility profiles, while also reducing the risk of over-prescription inherent in leaf-based replenishment models. Consequently, nutrient input decision-support frameworks can be validated via pour-through leachate analysis, organ-and whole-plant nutrient partitioning, and WUE

monitoring, providing a practical pathway to dynamic, physiologically grounded fertigation control throughout plant life cycles.

1.5 Toward Dynamic Nutrient Management

In containerized production systems, the pour-through leachate method enables non-destructive, time-resolved quantification of nutrient depletion from the root zone, thereby validating modeled uptake against cumulative solution loss and supporting dynamic recalibration of fertigation inputs through integrated monitoring of transpiration and solution nutrient depletion (e.g., Altland, 2021). Concurrently, continuous tracking of whole-plant transpiration and growth stage–dependent nutrient allocation provides a physiologically grounded basis for updating nutrient targets in situ and in real time, ensuring that nutrient delivery remains aligned with dynamic changes in water flux and whole-plant nutrient sink strength. Integrated systems that merge transpiration monitoring with solution depletion data can therefore potentially enhance NUE, reduce environmental losses, and optimize physiological performance under variable conditions (Ahmed et al., 2021).

1.6 Conclusion

Mass balance remains a rigorous, adaptable basis for nutrient management. Addressing the overlooked question of baseline uptake under non-limiting conditions, particularly in substrate systems, will be essential to advance organ-weighted accounting coupled with WUE-aware, sensor-driven control. By moving beyond static leaf targets toward whole-plant demand, mass balance can improve both agronomic performance and environmental stewardship. *C. sativa*, with its demonstrated propensity for luxury uptake in particular organs, provides an ideal model to refine these approaches and extend them to dynamic nutrient management across diverse crops.

2.1 Introduction

Despite rising fertilizer costs, nutrient delivery in hydroponic and containerized systems remains largely guided by empirically derived recipes rather than mechanistic understanding of elemental uptake. These formulations rarely reflect quantitative, element specific plant demand. As a result, this often leads to nutrient over-application, increased production costs, and elevated nutrient concentrations in leachate (Bugbee, 2004; Langenfeld & Bugbee, 2024; Sonneveld & Voogt, 2009). In addition, fixed recipes fail to account for dynamic changes in nutrient demand across genotype and developmental stages. This limitation can produce inaccurate elemental application and reduced sustainability(Bernstein et al., 2019; Caplan et al., 2018; Langenfeld et al., 2022; H. Marschner, 2012; Saloner & Bernstein, 2021).

Given the economic and regulatory importance of Cannabis sativa L. (C. sativa) production, there is a critical need for nutrient management strategies that align with physiological demand while minimizing environmental impact (Bernstein et al., 2019; Saloner & Bernstein, 2021). Mass balance approaches, grounded in the principle of elemental conservation, provide a quantitative framework for assessing nutrient uptake. Specifically, nutrient uptake is estimated as the difference between known nutrient inputs and measurable elemental accumulation in plant tissues (Bugbee, 2004; Langenfeld et al., 2022; Silberbush & Ben-Asher, 2001). When combined with measurements of nutrient depletion from the root-zone solution and organ-specific tissue concentrations, this framework allows total elemental uptake and intra-plant organ allocation to be quantified(Bugbee, 2004; Saloner & Bernstein, 2020; White & Brown, 2010). Although mass balance methods have been applied in several other crops, intraplant organ allocation has not been examined in C. sativa. This gap reflects, in part, the analytical demands associated with destructive sampling, tissue analysis, and precise fertigation monitoring(Konvalina et

al., 2024; Shiponi & Bernstein, 2021). Accordingly, the objective of this study was to evaluate organ specific and organ biomass-weighted mass balance frameworks for quantifying whole-plant nutrient uptake in high-value C. sativa production systems.

Plant acquisition of essential mineral elements occurs primarily from the rhizosphere (Cui, 2012; White & Brown, 2010), a process that can be quantified using mass balance principles to account for nutrient inputs and whole-plant storage (Cogley, 2010; Langenfeld et al., 2022). In controlled-environment systems, closed-loop fertigation supports steady-state nutrition, whereby water lost to transpiration is replaced with nutrient solution supplying elements taken up with that water (Langenfeld & Bugbee, 2024), thereby linking nutrient delivery to transpiration demand and improving nutrient-use efficiency (NUE). Within this framework, Langenfeld et al. (2022) computed irrigation solution element concentrations as the product of target leaf tissue concentrations and whole-plant water-use efficiency (WUE), yielding nutrient input concentrations (mg L^{-1}). Building on this approach, we apply an organ-explicit, biomass-weighted mass balance framework that links nutrient input calculations to developmental-stage uptake and transpiration driven water use and facilitates comparison between solution nutrient depletion with whole-plant nutrient uptake, which we evaluate using pour-through leachate analysis (Altland, 2021).

This study evaluated whether nutrient depletion from the fertigation solution corresponds to cumulative nutrient accumulation in discrete plant organs or whether organ biomass weighted accumulation more precisely reflects whole-plant nutrient uptake in relation to WUE dynamics. To address this question, we pursued four specific objectives. First, we quantified whole-plant nutrient uptake from solution depletion using pour-through leachate analysis. Second, we determined organ-specific element accumulation via ICP-OES. Third, we tracked cumulative water use and calculated whole-plant WUE. Fourth, we evaluated agreement between nutrient extraction from solution and both organ-explicit and biomass-weighted tissue concentration × WUE calculations used for fertigation recipe formulation. To our knowledge, this is the first study to directly compare organ-explicit and

organ biomass-weighted mass balance frameworks in C. sativa under controlled environment conditions. This work aims to advance resource-use efficiency in C. sativa production and to inform broader controlled-environment agriculture systems in which nutrient stewardship is essential for optimizing resource use and sustainability.

2.2 Materials and Methods

2.2.1 Plant Material and Clonal Propagation

This study evaluated the WUE and nutrient uptake dynamics of C. sativa cultivars 'CJ2' and 'First Light' using a mass balance approach. Lateral branch segments, 20 cm in length, were taken from mother plants for clonal propagation. On June 14, 2024, 1-inch rockwool cubes (Growdan, Milton, Ontario, Canada) were presoaked in deionized water (DI) containing a diluted complete fertilizer solution (17-5–17 Cal-Mag Special, Plant Marvel, Chicago Heights, Illinois, USA) at an electrical conductivity (EC) of 0.3 $dS \cdot m^{-1}$ adjusted to pH 6.0.

Each cutting was prepared by making a diagonal incision at the basal end with lower leaves removed leaving two nodes, followed by immersion in a rooting gel containing 3.3 g/L indole-3-butyric acid (Clonex, Growth Technology Ltd., Taunton, Somerset, UK). Cuttings were then inserted into the rockwool cubes. To minimize transpiration during root development, the leaves of each cutting were trimmed to approximately half their original surface area. A total of 16 cuttings (8 per cultivar) were propagated under a humidity dome on a 1020 horticultural tray. The tray was situated on a thermostatically controlled heat mat (Vivosun, 10" × 20.75", Ontario, California, USA) and illuminated continuously (24 h photoperiod) by a germination light fixture (Hydrofarm Jump Start T5, 61cm, Shoemakersville, Pennsylvania, USA). Daily misting with DI and periodic reapplication of 0.3 $dS \cdot m^{-1}$ fertilizer solution to the rockwool cube occurred until root development.

After 12 days, visible roots emerged from the rockwool cubes. The rooted cuttings were transplanted into 10 cm rockwool cubes presoaked in a complete fertilizer solution (17-5–17 Cal-Mag Special, Plant Marvel) with an EC of 1.0 mS/cm, and pH of 6.0. Plants

were then transferred to a growth chamber (Conviron, Model PG2500, Pembina, North Dakota, USA) and maintained under controlled conditions: 24-h photoperiod with a photosynthetic photon flux density (PPFD) of 340 $\mu mol \cdot m^{-2} \cdot s^{-1}$, air temperature of 22°C, and 40% RH. Over the following 10 days, chamber conditions were progressively increased to match those of the research greenhouse with an air temperature setpoint of 26.5°C and liquid feed provided to the plants at an EC of 1.0 $dS \cdot m^{-1}$ and pH of 6.0.

2.2.2 Greenhouse Experimental Design and Irrigation

Following environmental acclimation, the plants were moved to a research greenhouse at the Colorado State University Horticulture Center on July 7, 2024. The environmental conditions of the bay were adjusted via venting, forced air, and an end wall evaporative cooler to a set point of 26.5 °C, and natural gas heating set to initiate at 18.3°C. The vapor pressure deficit (VPD) varied over the experiment, with the majority of daily mean values between 1.2 and 1.6 kPa. Each cultivar was arranged in a single row of eight plants spaced 1.2 m between plants in the row and 1.5 m between the rows, totaling 16 plants. The rockwool cubes were transplanted into 11-L Bato buckets prefilled with 1.5 kg of dry horticultural grade perlite, which was selected due to its inability to chemically react with nutrient ions in solution.

To periodically deliver essential elements to the growing substrate, two dripper stakes per container delivered irrigation at a rate of 1.9 liter min^{-1} . Irrigation occurred at four daily intervals (0700, 1100, 1400, and 1900 h) for 10 minutes per cycle. The schedule was subsequently changed to two daily events (0700 and 2000 h) to establish an adequate uptake duration that was uninterrupted by irrigation events. To minimize substrate surface evaporative water loss, the surface of each container was covered with white plastic. Supplemental lighting was set to an 18/6-h (day/ night) photoperiod based on vegetative industry standards. The natural photoperiod at the time of the experiment's initiation was

14 h and 32 min calculated by the NOAA Solar Calculator (National Oceanic and Atmospheric Administration, n.d.).

After 16 days of initial growth in the greenhouse environment, essential elements were delivered via calibrated pneumatic pistons. The piston-driven injection system operates via compressed air which actuates individual element calibrated pistons to deliver fluid at a pressure setpoint maintained at 40 psi above the water pressure within the irrigation line. This ensures positive-pressure differential injection, enabling precise delivery of concentrated elements directly into an inline manifold to formulate a pre-determined complete recipe (nitrogen [N] - (nitrate – 250 ppm, ammonium 6.3 ppm), potassium [K] – 350 ppm, phosphorus [P] – 50 ppm, magnesium [Mg] – 61.7 ppm, calcium [Ca] – 100 ppm, iron [Fe] – 2 ppm, zinc [Zn] – 0.23 ppm, boron [B] – 0.09 ppm, copper [Cu] 0.23 ppm, molybdenum [Mo] – 0.07 ppm, manganese [Mn] – 0.27 ppm). The injection systems irrigation manifold was fitted upstream of a 113.5 L mixing tank, which supplied the 1.9 liter min^{-1} downstream dripper stakes with a complete nutrient solution

2.2.3 Gravimetric Water Use Measurements and Leachate Sampling

Gravimetric balances (Adam Equipment GBK-35A, Oxford, Connecticut, USA) were positioned under four representative plants per cultivar, in row positions 1, 3, 5, and 7 for ‘CJ2’, and 2, 4, 6, and 8 for ‘First Light’. Each balance was connected to a custom built IoT data acquisition system. The system consisted of a microcontroller (Adafruit ESP32 Feather, Brooklyn, New York, USA) powered by a lithium battery. The balance interfaces with data acquisition via an RS232 connection. Mass data were read and logged every 10 minutes via wireless transmission to a ThingSpeak dashboard (MathWorks, n.d.) for real-time monitoring and data storage.

Prior to substrate leachate extraction, substrate was watered to container capacity and allowed to drain for 30 minutes. Then, water transpired, measured continuously per container via gravimetric mass loss, was recorded throughout a 12 h day course. After 12 h

of nutrient solution uptake, the quantity of solution transpired was replaced with DI to return the substrate to container capacity. Resupplied DI was permitted to stabilize for 25 minutes. Thereafter, an additional mass of DI displacement solution was added to the substrate surface to hydraulically push 230 ml of solution out of the drainage elbow. During drainage, samples were filtered through 18×16 mesh screen, and the first 230 ml of the solution was collected in clean, unused bottles. We note that the volume of displacement solution collected (approximately 2% of container volume) was predetermined to obtain a representative sample of the bulk substrate rather than the bottom layer alone, given that leachate measurements were intended solely as an internal consistency check for comparing nutrient uptake with supplied inputs (Altland, 2021). Samples were immediately transferred to refrigerated storage for later analysis. Samples were collected every third day to ensure the substrate returned to base recipe stabilization prior to repeated extraction. A total of ten leachate sampling events occurred throughout the 38-day vegetative growth phase (July 7 – August 13, 2024).

2.2.4 Plant Measurements

Non-destructive individual plant biometric measurements of gravimetrically monitored plants were collected weekly. Stem caliper 5 cm above the rockwool surface was recorded as the average of two x and y direction caliper readings (mm). The height of the main stem was recorded as the distance from the surface edge of the Bato to the plant's terminal tip. Measurement of crown horizontal expansion was recorded as the average distance from the main stem in two perpendicular directions.

2.2.5 Biomass and Organ Tissue Analysis

After 38 days of vegetative growth monitoring, plants were destructively harvested. Immediately upon harvest, leaf area was quantified using a leaf area meter (LI-COR LI-3100, Lincoln, NE, USA). Root systems were carefully washed to remove perlite, then individual plant organs (leaves, stems, and roots) were dried at 70°C for ≥ five days until

constant mass. Dry mass per organ was recorded, and organ specific tissue was homogenized using a masticating grinder to obtain replicate plant organ tissue samples of approximately 5 g (n = 4) per cultivar. Organ specific tissue element analysis occurred via Thermo iCAP PRO EPS Duo ICPOES and NO_3^- was quantified by flow injection analyzer (FIA; FIAlyser-2000, FIAlab) (Brookside Laboratories, New Breman, Ohio, USA).

2.2.6 Nutrient Solution Input Concentration Estimation

Mass balance estimates of the individual element concentration required in nutrient solution were derived as described in Langenfeld et al. (2022). The predicted nutrient input concentration is the product of tissue element concentration (Equation 1) and plant WUE (Equation 2) where:

$$C_{input} = C_{tissue}\ x\ WUE \quad (1)$$

Mean tissue nutrient concentration (C_{tissue}) per organ was determined via ICP-OES analysis and used in combination with WUE to estimate individual element concentrations (C_{input}) within the nutrient solution.

WUE was calculated as:

$$WUE = \frac{M_{Dry}}{V_{irrigation}} \quad (2)$$

where (M_{Dry}) is total plant dry biomass (g $plant^{-1}$) and ($V_{irrigation}$) is the total irrigation volume transpired per plant (L $plant^{-1}$).

To estimate the whole-plant nutrient concentration, an organ biomass-weighted mean was calculated by its fractional contribution to the total biomass and then summed across all organs using the following equation:

$$C_{weighted} = \sum(C_{organ} X \frac{Biomass_{Organ}}{Biomass_{Total}}) \quad (3)$$

where ($C_{weighted}$) is the whole-plant biomass-weighted mean, (C_{organ}) represents the nutrient concentration measured in each individual organ (leaf, stem, root, or flower), ($Biomass_{organ}$) is the dry biomass of the organ, and ($Biomass_{total}$) is the total above and below-ground plant biomass. This approach integrates organ specific nutrient concentrations with their proportional contribution to total biomass, providing a physiologically meaningful estimate of the average whole-plant concentration. In effect, organs with greater biomass exert more influence on the weighted value, allowing the calculation to more accurately represent the nutrient status of the entire plant rather than relying on a single tissue type.

2.2.7 Statistical analysis

Elemental uptake data were analyzed using repeated measures analysis of variance (RM-ANOVA), with cultivar as a between subjects factor and date as a within-subjects factor. Data were organized by element, and each element was analyzed independently. The models were implemented using the ezANOVA function from the ez package in R (R Foundation for Statistical Computing, 2024), specifying replicate as the subject identifier to account for repeated observations. All categorical variables were converted to factors prior to analysis.

For each element, post hoc pairwise comparisons were conducted using estimated marginal means with the emmeans package. Bonferroni adjustment was applied to control the familywise error rate. Summary statistics, including means and standard errors, were computed for each cultivar × date combination and used to construct interaction plots.

Model assumptions were evaluated using residual diagnostics, and potential influential observations were identified using Cook's distance and leverage diagnostics from

the base lm function. All statistical analyses were performed in R (R Foundation for Statistical Computing, 2024), with significance determined at the a = 0.05 level.

Cultivar differences in tissue nutrient concentrations during the vegetative phase were evaluated using Welch's two-sample t-tests implemented in R (R Foundation for Statistical Computing, 2024). Analyses were conducted separately for each element and tissue (leaf, stem, root, and biomass-weighted mean), using replicate plants (n = 4 per cultivar) as the experimental unit. Welch's test was selected to accommodate unequal variances and small sample sizes. Mean values and standard errors were calculated from replicate-level observations, and statistical significance was assessed using two-tailed tests with a level of 0.05. All analyses and figure generation were fully scripted to ensure reproducibility.

2.3 Results

Plants were clonally propagated beginning on 14 June 2024 and transferred to the research bay on 7 July 2024. Following transfer, a short establishment period was allowed to permit root systems to acclimate to the experimental containers and nutrient solution within the containers to stabilize before initiating leachate-based measurements. As a result, nutrient uptake and gravimetric water use data collection commenced on 24 July 2024 and continued through 13 August 2024. Figures 1 and 2 therefore depict the active measurement period (day of year 206–225), while the vegetative phase described here includes both the establishment and subsequent monitoring intervals.

Figure 1 shows the cultivar difference in element uptake for N, K, P, Ca, and Mg. Cultivar-specific uptake patterns were present: N: ranged from 97–144 mg L^{-1} (First Light) and 75–135 mg L^{-1} (CJ2); K: from 112–216 mg L^{-1} and 106–205 mg L^{-1} ; P: from 14–47 mg L^{-1} and 12–47 mg L^{-1} ; Ca: from 44–97 mg L^{-1} and 37–96 mg L^{-1} ; and Mg: from 31–52 mg L^{-1} and 24–51 mg L^{-1} , respectively. Moreover, the initial three leachate collections showed significant variation between cultivars, however, cultivar differences diminished thereafter (Figure 1). WUE was similar between cultivars (CJ2: 4.71 g L^{-1} H 2 O; First Light: 4.59 g L^{-1}

H 2 O). Temporal analysis normalized to transpired water showed peak N and K uptake during week 1, with significant declines by week 2 ($p < 0.001$), while Ca and Mg uptake increased steadily over time ($p < 0.0001$).

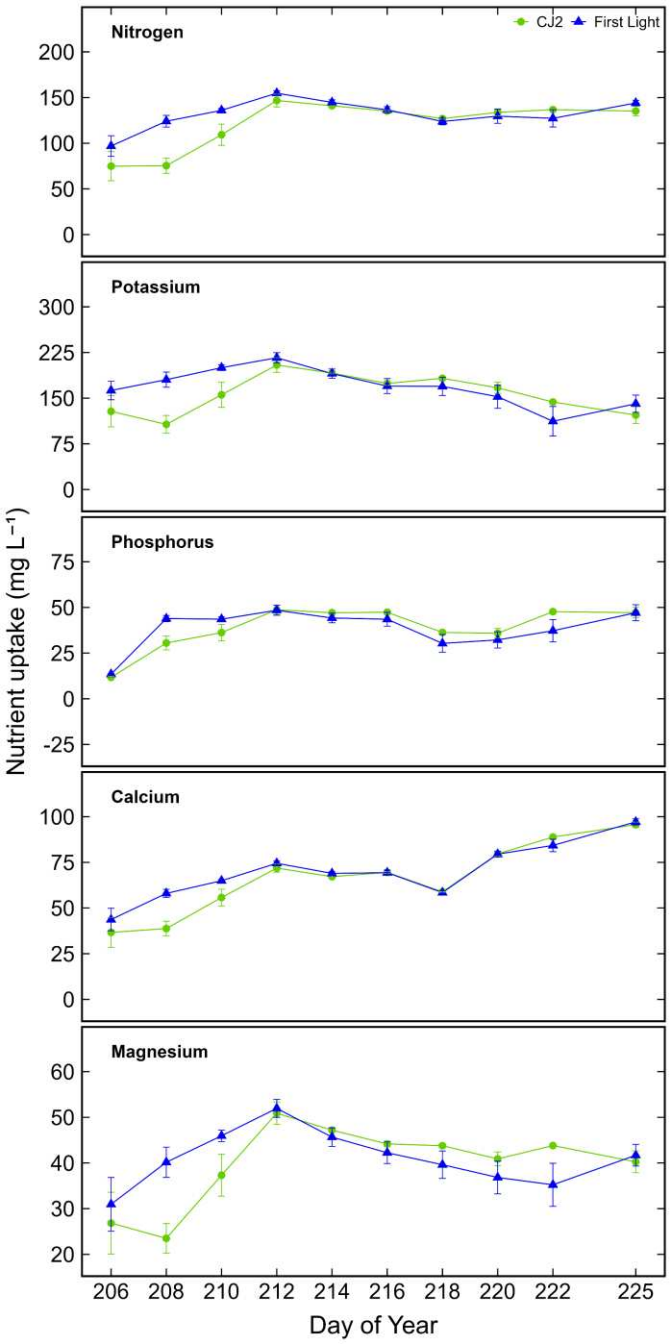

Figure 1 Calcium, magnesium, nitrogen, phosphorus, and potassium uptake from solution for cultivar CJ2 and First Light over ten repeated measure 12 h day uptake cycles over the course of the vegetative phase ± standard error of the mean. Data shown correspond to the active leachate sampling period following plant establishment.

Figure 2 shows the cultivar difference in element uptake for B, Cu, Mn, Fe, and Zn. Unlike macroelement uptake differences between cultivars, B, Cu, Mn, Fe, and Zn, showed little variation in uptake quantities between cultivars (Figure 2). For minor elements, CJ2

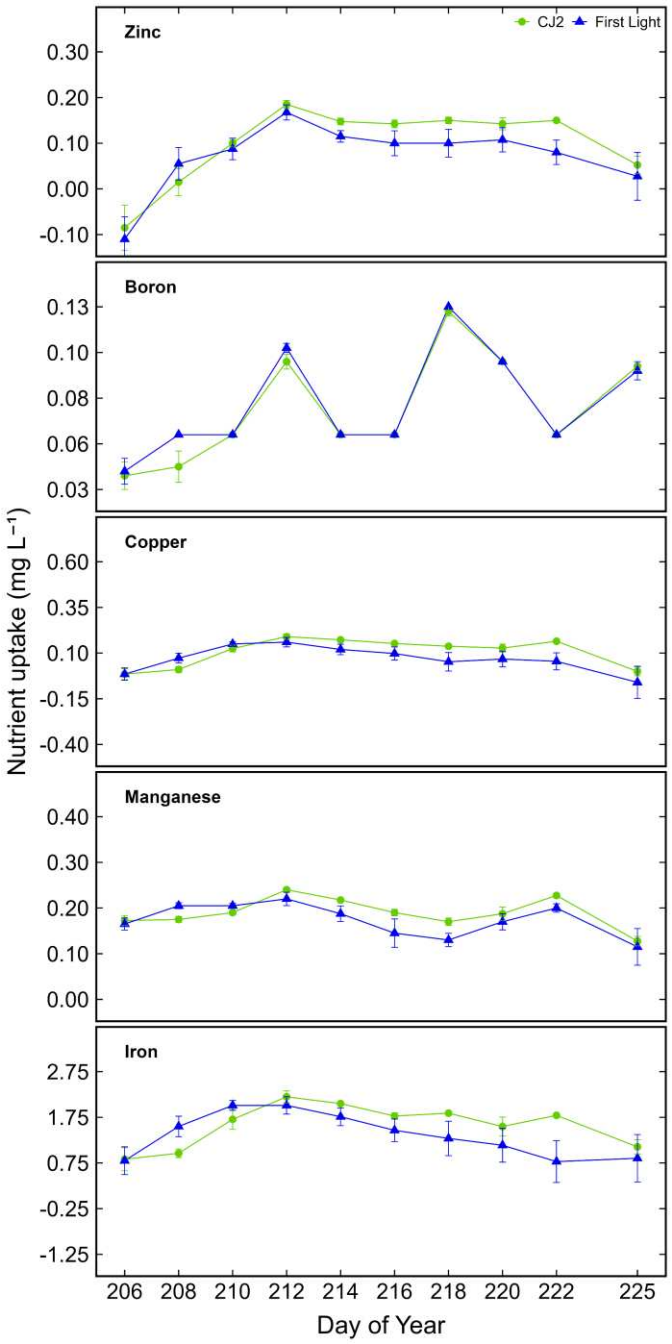

Figure 2 Boron, copper, iron, manganese, and zinc uptake from solution for cultivar CJ2 and First Light over ten repeated 12 h day uptake cycles over the course of the vegetative phase ± standard error of the mean. Data shown correspond to the active leachate sampling period following plant establishment.

and First Light also exhibited similar nutrient element extraction patterns when averaged across the monitored vegetative growth phase ($P > 0.05$) and cultivar differences in element uptake were not significantly different for most elements. However, repeated measures ANOVA revealed a significant effect of collection date ($P < 0.001$) for all 10 elements assessed, illustrating that uptake dynamics varied significantly throughout the 10 vegetative phase sampling intervals.

For macronutrients such as N, P, Ca, and P, a significant cultivar × date interaction was detected ($P < 0.05$), indicating that the cultivars responded differently to nutrient supply over time. Bonferroni's post hoc comparisons showed that in early vegetative stages, CJ2 had consistently higher N and K uptake as compared to First Light, though differences declined later in the vegetative stage. For example, on July 24, N uptake for CJ2 exceeded that of First Light by 25% ($P = 0.014$). Linear mixed-effects models supported the stability of these findings after controlling for potential outlier influence, showing no significant differences between cultivars in total element uptake over time for Zn, Fe, Mn, and Cu, although all exhibited significant temporal variation in uptake ($P < 0.001$) consistent with additional extraction as biomass increased. The element uptake per unit of H_2O transpired did provide an estimate of the daily nutrient replenishment amounts required to maintain stable nitrate and potassium concentrations in the input nutrient solution.

Mean nutrient uptake from solution for each cultivar was compared to predicted concentrations derived from leaf, stem, and root tissues, as well as organ biomass-weighted means (Table 1). The accuracy of each prediction varies by cultivar, element, and organ. For N, the organ-weighted mean most closely matched solution uptake in CJ2 and First Light, with deviations of +2.9% and – 3.1%, respectively. Leaf tissue consistently overpredicted N uptake (34.3% in CJ2; 25.6% in First Light), while root values underpredicted uptake in both cultivars by 19.4% and 5.9%. Stem predictions were the least accurate, underestimating nutrient uptake by 36.3% (CJ2) and 37.3% (First Light). P uptake was best predicted by root tissue concentrations in both cultivars, with a small overprediction of 7.5%

(CJ2) and underprediction of 20.3% (First Light). Stem P values were again least accurate, underpredicting solution uptake by 65.8% in CJ2 and 59.2% in First Light. Organ-weighted means also underpredicted P uptake by 51% (CJ2) and 46.5% (First Light). For K, solution uptake was best predicted by the root tissue element concentration in CJ2 (–26.6%). First Light stem values, on the other hand, were the closest to predicting potassium uptake (–19.7%), however, stem concentrations underpredicted K uptake in CJ2 (29.7%). Ca uptake was best approximated by the organ biomass-weighted mean in CJ2 (–15.8%) and by the leaf concentration in First Light (–4.5%), the latter representing the most accurate prediction for any tissue in that cultivar. In First Light, however, the organ biomass-weighted mean underpredicted by 27.7%, whereas in CJ2 the stem underpredicted Ca uptake by 54.7%, and leaf values overestimated uptake for CJ2. For Mg, uptake was best predicted by the leaf concentration in both First Light (–31.2%) and CJ2 (–4.7%), which more closely matched nutrient solution uptake than either stem or root estimates. In both cultivars, root predictions significantly underpredicted Mg uptake; CJ2 (42.7%) and First Light (43.1%) and stem estimates were the least accurate, deviating by –74.4% (CJ2) and –72.3% (First Light). Organ biomass-weighted means were intermediate at –38.3% and –49.8% in CJ2 and First Light, respectively. Fe uptake was generally underpredicted by leaf, stem and organ weighted values in both cultivars. The root mean concentrations predicted approximately twice the amount of measured uptake in both cultivars, overpredicting 88.6% (CJ2) and 108% (First Light). Stem values underpredicted Fe uptake by ~88% in both cultivars and were less accurate than leaves, whereas the organ-weighted mean value came the closest to uptake values at –63.3% and –55.5% for CJ2 and First Light (Table 1).

Table 1. Mean boron [B], copper [Cu], calcium [Ca], iron [Fe], magnesium [Mg], manganese [Mn], nitrogen [N], phosphorus [P], potassium [K], and zinc [Zn] uptake from solution for cultivar CJ2 and First Light for ten repeated measures of 12 h day uptake cycles over the course of the vegetative phase. Uptake from solution (Uptake) for cultivar CJ2 and First Light and organ-explicit (leaf, stem, and root) and organ biomass-weighted (Weighted) mass balance calculations in relation to water use efficiency dynamics. Values are the mean of four replicate plants per cultivar averaged over ten repeated 12 h day uptake cycles ± standard error of the mean.

	Uptake (ppm)	Leaf (ppm)	Stem (ppm)	Root (ppm)	Weighted (ppm)
CJ2					
N	121.52 ± 5.56	163.14 ± 10.34	77.51 ± 16.28	145.08 ± 5.50	125.08 ± 11.99
P	38.86 ± 1.89	19.84 ± 1.29	13.28 ± 1.67	35.94 ± 1.60	19.00 ±1.62
K	157.62 ± 10.40	75.25 ± 4.00	110.83 ± 12.14	115.67 ± 11.14	94.76 ± 7.19
Ca	66.27 ± 2.36	84.04 ± 7.64	30.04 ± 7.30	35.99 ± 2.89	55.78 ± 6.84
Fe	1.58 ± 0.12	0.36 ± 0.03	0.15 ± 0.03	2.98 ± 0.24	0.58 ± 0.07
Mg	39.86 ± 2.25	37.98 ± 3.12	10.20 ± 2.02	22.83 ± 1.46	24.60 ± 2.39
Mn	0.19 ± 0.01	0.20 ± 0.02	0.23 ± 0.03	0.37 ± 0.03	0.23 ± 0.02
B	0.07 ± 0	0.13 ± 0	0.05 ± 0.01	0.05 ± 0	0.08 ± 0.01
Cu	0.11 ± 0.02	0.01 ± 0	0.03 ± 0.02	0.05 ± 0	0.02 ± 0.01
Zn	0.10 ± 0.02	0.10 ± 0.01	0.04 ± 0.01	0.10 ± 0	0.08 ± 0.01
First Light					
N	131.77 ± 5.25	165.60 ± 2.39	82.58 ± 6.89	139.53 ± 1.72	127.70 ± 2.46
P	38.40 ± 3.21	21.70 ± 0.44	15.69 ± 1.05	30.62 ± 1.39	20.56 ± 0.51
K	169.41 ± 13.30	77.74 ± 2.00	135.90 ± 9.54	105.29 ± 4.08	105.70 ± 3.28
Ca	69.89 ± 2.02	66.76 ± 1.66	40.54 ± 5.55	29.83 ± 2.11	50.50 ± 2.04
Fe	1.37 ± 0.30	0.27 ± 0.01	0.17 ± 0.02	2.85 ± 0.32	0.61 ± 0.04
Mg	41.03 ± 3.05	28.23 ± 0.57	11.36 ± 1.28	23.35 ± 0.88	20.58 ± 0.55
Mn	0.17 ± 0.02	0.27 ± 0.01	0.17 ± 0.02	0.34 ± 0.03	0.24 ± 0.01
B	0.08 ± 0	0.09 ± 0	0.06 ± 0.01	0.05 ± 0	0.07 ± 0
Cu	0.07 ± 0.04	0.01 ± 0	0 ± 0	0.04 ± 0	0.01 ± 0
Zn	0.07 ± 0.03	0.09 ± 0	0.04 ± 0	0.10 ± 0	0.07 ± 0

For Mn, leaf values were the most accurate predictor of uptake in CJ2, with a deviation of only +5.3%, whereas the stem value was an exact match of measured uptake in First Light (0.17 ppm). The organ biomass-weighted mean overestimated uptake in CJ2 (21.1%) and First Light (41.2%), while root values in both cultivars (0.34–0.37 ppm) overpredicted by almost twice that of actual uptake from solution. For B, uptake was most accurately predicted by the organ biomass-weighted mean in CJ2 (+14.3%) and by either the leaf or organ biomass-weighted mean values in First Light (± 12.5%), whereas stem and root concentrations underestimated uptake by approximately 30% in both cultivars. Cu was generally underpredicted; however, the root values were the closest to measured uptake in CJ2 and First Light, respectively. Stem Cu concentrations were consistently low (<0.01 ppm) and did not closely align with uptake values in either cultivar. Both leaf and root calculated input values (0.10 ppm) were exact matches for Zn uptake from solution (0.10 ppm) in CJ2. In First Light, alternatively, the organ biomass-weighted mean matched the uptake value (0.07 ppm)

Figure 3 presents cultivar comparisons of macro-element input solution concentrations calculated for each organ and as organ biomass-weighted means. With the exception of four cases, organ specific and biomass-weighted concentrations were not significantly different. Four macro-elements exhibited cultivar-level divergence for root phosphorus, stem potassium, leaf calcium and magnesium. Nonetheless, between cultivar differences were not significant.

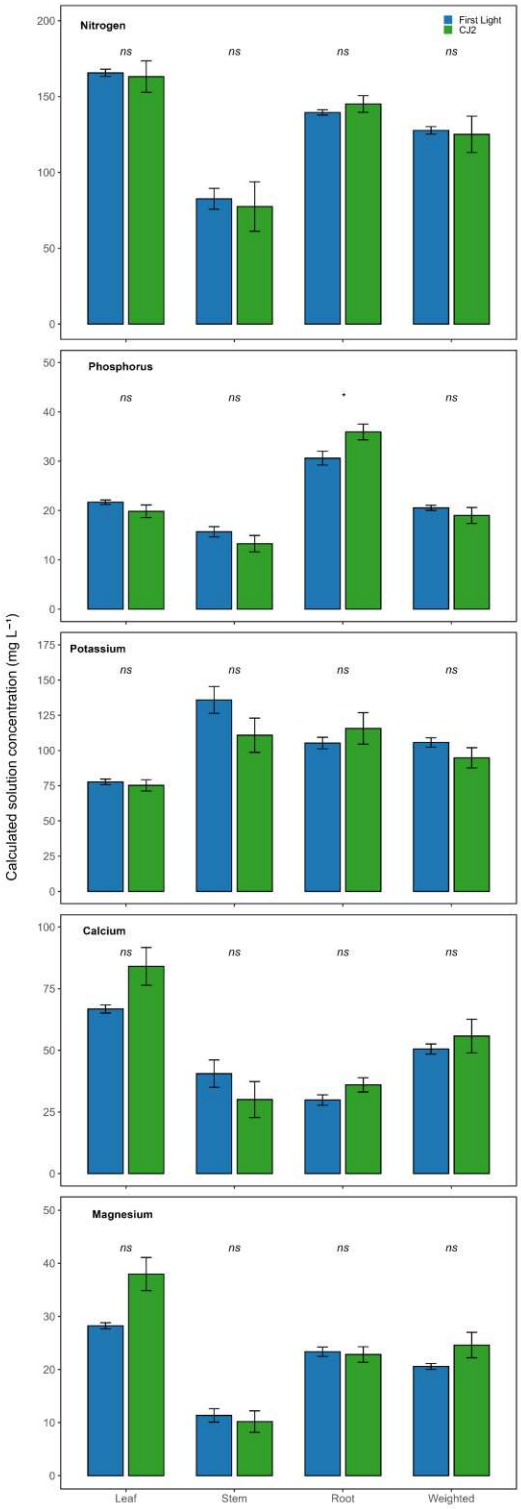

Figure 3 Comparison of calculated mean solution input concentrations derived from leaf, stem, root, and organ biomass-weighted tissue measurements for calcium, magnesium, nitrogen, phosphorus, and potassium in cultivars CJ2 and First Light (n = 4). Bars represent time-averaged means ± standard error across the vegetative monitoring period. "ns" denotes no significant cultivar main effect ($P \geq 0.05$) based on repeated-measures ANOVA.

Figure 4 shows the corresponding micro-element comparisons. Substantial cultivar differences were observed in seven cases. These involved leaf boron, manganese, and zinc; stem and root copper; and the biomass-weighted concentrations of boron and copper. Although mean differences between cultivars appear visually distinct for some elements and tissues in Figures 3, 4, these patterns were not consistently supported by statistical separation. Apparent differences in bar height reflect numerical differences in cultivar means, whereas statistical inference additionally accounts for variability among replicate plants and the resulting uncertainty around the means. For elements such as calcium and magnesium, relatively large within-cultivar variation reduced the ability to distinguish cultivar effects despite observable mean separation. Consequently, these comparisons are interpreted as numerical trends rather than statistically robust differences. In contrast, significant cultivar differences were observed for several micronutrients. Figure 4 illustrates where they are both visually apparent and statistically supported, highlighting that cultivar differences during the vegetative phase were element- and tissue specific rather than uniform across nutrients.

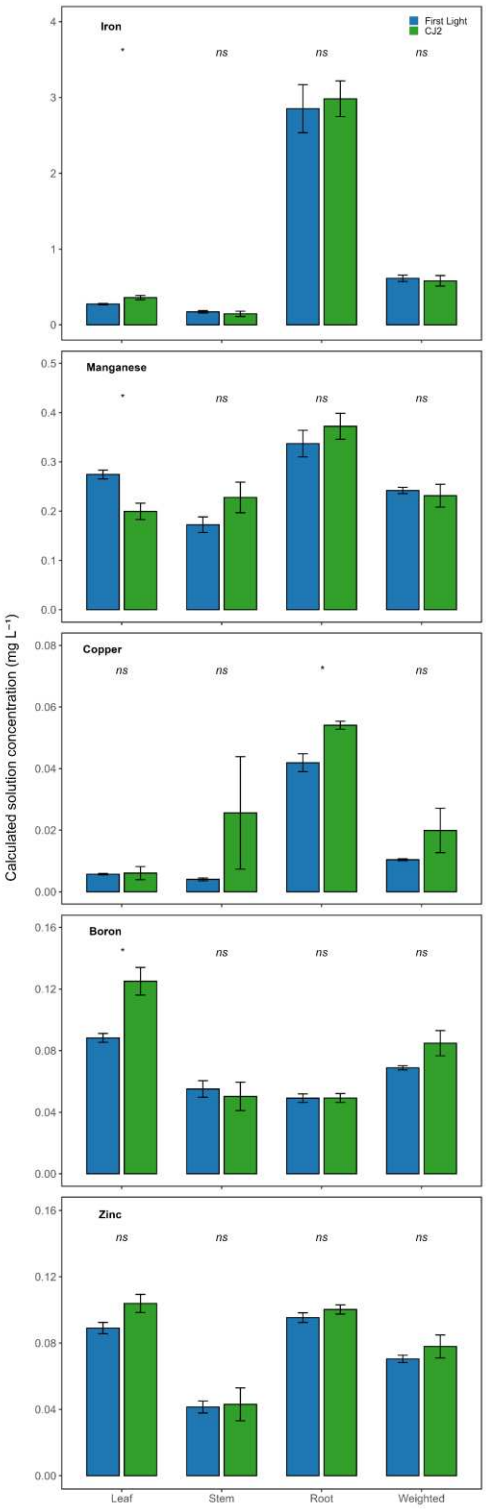

Figure 4 Comparison of calculated mean solution input concentrations derived from leaf, stem, root, and organ biomass-weighted tissue measurements for boron, copper, iron, manganese, and zinc in cultivars CJ2 and First Light (n = 4). Bars represent time-averaged means ± standard error across the vegetative monitoring period. "ns" denotes no significant cultivar main effect ($P \geq 0.05$) based on repeated-measures ANOVA.

2.3. Discussion

2.3.1 Introduction

A core principle of the mass balance framework is that absorbed elements retain their atomic identity throughout the plant's life cycle, enabling quantitative inference of nutrient inputs from tissue composition and transpiration metrics. This biochemical constancy underpins the robustness of the mass balance approach and is consistent with established stoichiometric principles in plant systems (Balboa et al., 2018).

2.3.2 Mass Balance and Cultivar-Specific Uptake Dynamics

By aligning nutrient input with water use, the mass balance framework supports precise, physiology-based fertigation strategies and builds on prior work in hydroponic systems (Hershkowitz et al., 2025; Langenfeld et al., 2022; Westmoreland & Bugbee, 2022). To evaluate whether nutrient depletion from the fertigation solution reflects physiological demand, nutrient supply was intentionally maintained above uptake throughout the vegetative phase, allowing direct comparison between measured nutrient uptake from solution and mass balance predictions. Observed nutrient uptake generally exceeded published sufficiency ranges, consistent with reports of luxury consumption in vegetative *C. sativa* that does not necessarily enhance yield (Saloner & Bernstein, 2020, 2021; Shiponi & Bernstein, 2021; Westmoreland & Bugbee, 2022). Despite similar WUE between cultivars CJ2 (4.71 g L^{-1} H_2O) and First Light (4.59 g L^{-1} H_2O), distinct uptake patterns emerged during early growth. CJ2 exhibited significantly greater N and K uptake in the first week (Figure 1), with N uptake exceeding that of First Light by 25% on day of year 206 (July 24) ($P = 0.014$), consistent with genotypic variation in root development, nutrient transport efficiency, and internal demand (H. Marschner, 2012; Xu et al., 2012). Repeated measures ANOVA confirmed significant cultivar × date interactions for N, P, K, and Ca ($P < 0.05$), but not for Fe, Mn, Cu, or Zn, whose uptake patterns converged across cultivars over time (Figure 2). These results indicate that macronutrient demand is more genotype-

dependent, while micronutrient uptake is increasingly driven by biomass accumulation and transpiration-mediated mass flow in later stages (Bugbee, 2004).

2.3.3 Organ-Specific vs. Whole-Plant Nutrient Estimates

Across all elements measured in this study, no single tissue consistently provided the best prediction of nutrient uptake from solution in either cultivar. The organ biomass-weighted mean was the most accurate predictor for N (both cultivars), Ca (CJ2), B (CJ2), and Zn (First Light). Leaf tissue most accurately predicted uptake of Mg (CJ2), Mn (CJ2), and Zn (CJ2). Root tissue concentrations best predicted uptake of P (both cultivars), K (CJ2), Cu (both cultivars), and Zn (CJ2), while also providing the second-best estimates in multiple instances. Leaf values were the best predictors for Ca (First Light) and stem values were the best predictors for Mn (First Light). These findings demonstrate that while individual organ means can perform well, element and cultivar-specific patterns exist, and root or even stem concentrations can sometimes be the most accurate predictors as compared to leaf concentrations. Therefore, multi-organ assessment remains valuable when precise nutrient demand estimation is required for optimizing fertigation strategies.

This organ-specific variability aligns with prior work showing that reliance on leaf tissue analysis alone can misrepresent whole-plant nutritional status, particularly for mobile macronutrients such as N, K, and Mg. Redistribution of these nutrients among organs is well documented, especially when plants mobilize resources toward developing tissues (Ingestad, 1982; Juarez-Maldonado et al., 2017). Recent meta-analyses confirm that integrating nutrient concentrations across organs, weighted by their respective biomass, yields a more accurate representation of whole-plant nutrient status than single-organ measurements (Sperling, 2020).

Our findings reflect this complexity. The organ biomass-weighted mean consistently provided the most accurate predictions for N, Ca, B, and Zn uptake, closely matching measured solution depletion values across both cultivars. For P, K, and Cu, root

concentrations offered the best match, while leaf concentrations were most accurate for Mg in certain cases. No single organ type consistently predicted element uptake for all elements or cultivars, underscoring the element and genotype-specific nature of nutrient partitioning.

These results demonstrate that organ biomass-weighted means, in combination with targeted organ measurements where appropriate, offer the most robust approach for inferring whole-plant nutrient demand in mass-balance fertigation models. Accordingly, multi-organ sampling remains essential for accurate calibration and for minimizing bias in nutrient budgeting.

2.3.4 Broader Implications and Operational Considerations

While the static measurement of WUE and tissue concentrations in this study captures a snapshot of nutrient–water dynamics, it lacks the temporal resolution necessary to capture shifting nutrient demand throughout the vegetative growth stage. Prior studies have demonstrated that seasonal and ontogenetic changes can substantially alter nutrient uptake patterns, indicating that repeated biomass and transpiration measurements would improve model fidelity (Juarez-Maldonado et al., 2017). Implementing mass balance strategies also requires precise quantification of water use and organ-level nutrient accumulation, more feasible in controlled environments than in open-field systems. However, the increasing use of closed-loop systems with real-time monitoring capabilities provides an ideal platform for adaptive fertigation management (Houston, 2021).

Mass balance models present a compelling alternative to fixed nutrient recipes by enabling feedback-driven fertigation protocols. This is particularly advantageous in high-value crops such as *C. sativa*, where genotype-specific nutrient demands are pronounced. In semi-closed or zero-discharge systems, these approaches can minimize nutrient loss and environmental impact by precisely matching supply to uptake.

2.4 Conclusions

This study provides preliminary evidence that a mass-balance framework can estimate nutrient uptake in C. sativa. By integrating transpiration-driven water flux with tissue nutrient concentrations, we derived empirically supported estimates of nutrient uptake per unit of water transpired. This integration allows irrigation nutrient solution input concentrations to be estimated to correspond with plant uptake. Critically, the results also highlight the limitations of relying solely on single-organ nutrient concentrations, particularly leaf tissue, for predicting whole-plant nutrient status. Given the substantial differences in elemental concentrations among roots, stems, and leaves, an organ-inclusive, biomass-weighted approach provides a more accurate whole-plant estimate (He et al., 2015; Jiang et al., 2024; Jing et al., 2020; Tang et al., 2018).

By linking nutrient inputs to transpiration and tissue accumulation, this framework facilitates closed-loop feedback control, enabling fertigation to be dynamically adjusted in response to actual plant uptake. Such adaptive protocols enhance resource use efficiency, reduce nutrient waste, and minimize environmental impact, particularly in recirculating hydroponic and semi-closed systems (Houston, 2021; Langenfeld et al., 2022).

3.1. Introduction

Predominantly, nutrient solution concentrations are determined by fertilizer compositions rather than plant uptake dynamics or physiological demand, often relying on electrical conductivity (EC) proxies instead of ion-specific control (Fathidarehnijeh et al., 2023; Sulaiman et al., 2025). This can lead to excessive or imbalanced fertilization, which undermines precision and sustainability. The high production costs of controlled environments, combined with the economic value of *Cannabis sativa* L. (*C. sativa*), make this crop particularly susceptible to excessive fertilizer application (Cockson et al., 2020; Saloner & Bernstein, 2022, 2023). As fertilizer costs rise and mineral reserves become increasingly limited, aligning nutrient supply with actual plant demand is essential for both economic viability and sustainable resource use (Fuentes-Peñailillo et al., 2024).

Transpiration is a biologically regulated physical process that links water and nutrient fluxes. Because evaporative demand drives xylem mass flow, ions are delivered to organs at rates modulated by water-use efficiency (WUE), which links environmental conditions to transpiration-driven nutrient budgeting. A justifiable fertigation strategy is to replace water and ions removed by plants rather than maintain constant element setpoints within solution (Bugbee, 2004; Langenfeld et al., 2022; Langenfeld & Bugbee, 2024). This shifts nutrient management from static concentration control to dynamic flux replacement, a need that intensifies as nutrient uptake and partitioning change after floral initiation (Hershkowitz et al., 2025; Massuela et al., 2023; Westmoreland & Bugbee, 2022). Flux-based replacement inherently aligns fertigation with physiological demand and developmental dynamics, improving precision, sustainability, and the efficient use of increasingly scarce mineral and freshwater resources (Fuentes-Peñailillo et al., 2024; Hershkowitz et al., 2025).

Following floral initiation, biomass allocation in *C. sativa* shifts toward reproductive structures, lowering the root: shoot ratio as inflorescences expand (Saloner & Bernstein,

2023). This transition modifies nutrient demand and mobility: calcium uptake declines late in flowering despite ongoing floral growth, whereas phosphorus, potassium, and magnesium translocation increases (Saloner & Bernstein, 2023). These dynamics underscore the limitations of static nutrient recipes and the need for stage-specific, flux-based supply. Similar discrepancies between balance-derived uptake and tissue estimates occur in tomato for nitrogen, magnesium, and sulfur (Cedeño et al., 2024). Because mass flow governs delivery of ions with limited phloem mobility, environmental effects on WUE directly influence transport (Langenfeld et al., 2022; Massuela et al., 2023). Incorporating WUE into mass-balance calculations therefore provides a robust basis for adjusting nutrient supply across environments and developmental stages (Langenfeld et al., 2022; Massuela et al., 2023; Sperling et al., 2020).

Reproductive-phase fertigation in *C. sativa* remains insufficiently resolved because nutrient composition, WUE, and ion-uptake dynamics have rarely been integrated into a unified framework (Cedeño et al., 2024; Saloner & Bernstein, 2023; Westmoreland & Bugbee, 2022). Most studies emphasize single nutrient concentration targets rather than coupling tissue elemental requirements to water-driven mass flow. The present work closes this gap by using a transpiration-driven mass-balance approach to quantify reproductive-stage nutrient depletion and/or accumulation in organ tissue and organ-specific biomass-weighted elemental composition measured water flux. This mechanistic framework links tissue element concentration and WUE directly to uptake-mediated depletion of nutrients and water from substrate solution, enabling the estimation of fertigation solution element replenishment rates that are constrained by both developmental shifts in nutrient uptake and partitioning and the biophysics of transpiration-driven xylem transport.

Accordingly, this study investigates: (i) how organ-level nutrient concentrations and whole-plant nutrient biomass-weighted elemental composition relate to changes in solution nutrient concentrations; (ii) how WUE adjusts nutrient concentrations in irrigation solutions to meet tissue-based requirements across environments, cultivars, and developmental

stages; and (iii) the extent to which leachate element composition corroborates or contradicts mass balance estimates of water removal and nutrient input replenishment concentrations. By integrating organ-weighted tissue element data with WUE, this work provides a reproducible procedure for calculating daily solution input replenishment recipes, defining cultivar-specific nutrient uptake profiles, and establishing a framework to distinguish reproductive-phase changes in organ- and whole-plant level nutrient requirements.

3.2. Materials and Methods

3.2.1 Plant Material and Clonal Propagation

Ninety cuttings (45 per cultivar) of two *C. sativa* cultivars, CJ2 and First Light, were excised and clonally propagated. On 9, August 2024, 1-inch rockwool cubes (Growdan, Milton, Ontario, Canada) were presoaked in deionized water (DI) containing a diluted complete fertilizer solution (12-2-12 Plug Special, Plant Marvel Chicago Heights, Illinois, USA) adjusted to an electrical conductivity (EC) of 0.3 $dS \cdot m^{-1}$ and pH 6.0. Each cutting was prepared by making a diagonal basal incision and dipping the base into a rooting gel containing indole-3-butyric acid (Clonex, Growth Technology Ltd., Taunton, Somerset, UK) before insertion into the rockwool. Leaves on each cutting were trimmed to approximately 50% of their original area to limit transpiration during rooting.

Cuttings were placed in 1020 trays in a growth chamber (Conviron, Model PG2500, Pembina, North Dakota, USA). Chamber environmental conditions were 24 h photoperiod at 340 $\mu mol \cdot m^{-2} \cdot s^{-1}$ photosynthetic photon flux density (PPFD), 22°C air temperature, and 80% relative humidity (RH). The cubes were remoistened periodically with the fertilizer solution. After 10 days, plants were moved to a research bay at the Colorado State University Horticulture Center. Environmental conditions of the bay were controlled via venting, forced air, and an end wall evaporative cooling system to maintain an air temperature set point of 26.5 °C, and natural gas heating set to initiate at 18.3 °C. Vapor pressure deficit (VPD) varied throughout the experiment, with the majority of daily mean

values between 1.2 and 1.6 kPa. Supplemental lighting was initially set to an 18/6-h (day/night) photoperiod based on vegetative industry standards and supported by literature by (Ahrens et al., 2023). Roots emerged after one week. After 18 days from excision, 23 vigorous plants per cultivar were chosen for growth uniformity and transplanted into 4-inch rockwool cubes (Growdan, Milton, Ontario, Canada) pre-soaked in a complete fertilizer solution (EC 1.0 $dS \cdot m^{-1}$, pH 6.0). On September 1, these planted 4-inch cubes, 46 in total, were seated into pre-positioned 11-L Bato buckets (CropKing Inc., Lodi, Ohio, USA) filled with 1.5 kg oven dry horticultural perlite, which was selected due to its inert cation exchange capacity characteristics that make it ideal for its inability to chemically react with nutrient ions in solution.

3.2.2 Greenhouse Experimental Design and Fertigation

Fertigation was delivered via two dripper stakes at a rate of 1.9 $liter \cdot min^{-1}$. Essential elements were delivered via calibrated pneumatic pistons as described in (Powell & Bauerle, 2026). The nutrient input recipe contained the following elements: nitrogen [N] (nitrate – 250 ppm, ammonium - 6.3 ppm)), potassium [K] – 350 ppm, phosphorus [P] – 50 ppm, magnesium [Mg] – 61.7 ppm, calcium [Ca] – 100 ppm, iron [Fe] – 2 ppm, zinc [Zn] – 0.23 ppm, boron [B] – 0.09 ppm, copper [Cu] – 0.23 ppm, molybdenum [Mo] – 0.07 ppm, and manganese [Mn] – 0.27 ppm. Initially, fertigation was supplied four times daily (0700, 1100, 1500, and 2000 h). For the primary fertigation cycles, the duration was determined based on observed leachate at each fertigation event to ensure substrate saturation. The schedule was subsequently changed to two daily events (0700 and 2000 h). The time duration between the two daily fertigation events served as a closed system that was uninterrupted by fertigation events. To minimize substrate evaporative water loss, the surface of each container was covered with white plastic. To initiate flowering, supplemental lighting was switched on 10, September 2024 to a 12/12 photoperiod, a photoperiod known to change C. *sativa* from the vegetative to the reproductive phase. In addition, black plastic

was hung on the greenhouse wall adjacent to the research bay to prevent light pollution. Natural day length at this date was approximately 12 h 40 min (National Oceanic and Atmospheric Administration, n.d.), which was less than the dark period length required for *C. sativa's* reproductive phase (Ahrens et al., 2023).

3.2.3 Continuous Gravimetric Water-Use Measurements

Of the 23 replicate plants per cultivar, eight replicates were placed on independent gravimetric balances (Adam Equipment GBK-35A Milton Keynes, Buckinghamshire UK). The plants were positioned in a 5 x 8 matrix with 1.5 m inter-plant spacing. Each balance interfaced with a custom IoT data-acquisition system (Adafruit ESP32 Feather, lithium-battery powered) via RS-232. Mass measurements were transmitted every 10 min to a ThingSpeak dashboard for real-time visualization and data storage (MathWorks, n.d.).

Prior to substrate leachate extraction, the substrate was watered to container capacity and allowed to drain for 30 minutes. Then, water transpired, was recorded throughout a 12 h-day course. After 12 h, the quantity of solution transpired was replaced with an equal amount of deionized water (DI) to return the substrate to container capacity. Resupplied DI was permitted to stabilize for 25 minutes. Thereafter, following best practice pour through procedures described in Altland (2021), an additional mass of DI displacement solution was added to the substrate surface to hydraulically push 230 ml of solution out of the drainage elbow. During drainage, samples were filtered through 18×16 mesh screen, and the first 230 ml of solution was collected in clean, unused bottles. We note that the amount of displacement solution collected (approximately 2% of container volume) was predetermined to provide a sample that represents the entire bulk of the substrate, not just the bottom layer (Altland, 2021). Samples were immediately transferred to refrigerated storage for later analysis. Leachate sampling was conducted every tenth day for the duration of the reproductive phase (September 10 – November 9, 2024), yielding seven

closed-system sampling events of eight replicate leachate samples per cultivar throughout the reproductive growth phase.

3.2.4 Plant Uniformity Measurements

At 10-day intervals, morphological data were recorded for each of the 23 plants per cultivar. Stem caliper was measured at a consistent position 5 cm above the rockwool cube; two perpendicular readings (x and y) were averaged. Plant height was measured from the rim of the Bato bucket to the apex of the main stem. Canopy spread was quantified as the mean of orthogonal canopy diameters transversing the center perpendicular to one another.

3.2.5 Biomass and Organ Tissue Analysis

In conjunction with leachate sampling, destructive harvests were performed every 10 days beginning September 10, 2024, with the harvest of 6 plants (3 per cultivar). Plants were partitioned into leaves (defoliated), stems, roots (washed), and flowers (n = 3 per cultivar). At the first harvest following the photoperiod change (DFPC) to a 12/12 cycle (DFPC 0), and again at the subsequent harvest interval (DFPC 10), initial inflorescences had not yet developed sufficient biomass for reliable quantification. We note that at the time of each harvest the sugar leaves, floral peduncle leaves per inflorescence, were excised then pooled along with the defoliated leaves Leaf area was measured using a leaf area meter (LI-COR LI-3100, Lincoln, NE, USA). All tissues were oven-dried at 70 °C for ≥5 days to constant mass, then dry weights were recorded.

Organ specific tissue was masticated per replicate per cultivar using a stainless-steel grinder. Samples (5g) were then collected from each replicate organ for an overall organ representation per plant and sent for analysis via Thermo iCAP PRO EPS Duo ICP-OES and NO_3^- was quantified by flow injection analyzer (FIA; FIAlyser-2000, FIAlab) (Brookside Laboratories, New Breman, Ohio, USA).

3.2.6 Nutrient Solution Input Concentration Estimation via Mass Balance

A mass-balance-based approach was used to estimate individual element solution replacement concentrations as described in Langenfeld et al. (2022). The nutrient mass balance procedure assumes that nutrients in a closed system are either in the nutrient solution or in the plant tissue. The predicted nutrient replacement input concentration for each essential nutrient is the product of organ tissue element concentration and the rate at which nutrients are removed from solution i.e. the plant WUE where:

$$C_{input} = C_{tissue}\ x\ WUE \qquad (1)$$

As previously described, mean tissue concentration (C_{tissue}) per organ was determined via ICP-OES analysis and/or flow injection analysis and used in combination with WUE to estimate optimal individual element input concentrations (C_{input}) within the nutrient solution.

WUE was calculated as:

$$WUE = \frac{M_{Dry}}{V_{irrigation}} \qquad (2)$$

where (M_{Dry}) is total plant dry biomass (g plant^{-1}) and ($V_{irrigation}$) is the total irrigation volume transpired per plant (L plant^{-1}).

where ($C_{weighted}$) is the whole-plant biomass-weighted mean, (C_{organ}) represents the nutrient concentration measured in each individual organ (leaf, stem, root, or flower), ($Biomass_{organ}$) is the dry biomass of the organ, and ($Biomass_{total}$) is the total above and below-ground plant biomass.

$$C_{weighted} = \sum(C_{organ} X \frac{Biomass_{Organ}}{Biomass_{Total}}) \quad (3)$$

where ($C_{weighted}$) is the whole-plant biomass-weighted mean, (C_{organ}) represents the nutrient concentration measured in each individual organ (leaf, stem, root, or flower), ($Biomass_{organ}$) is the dry biomass of the organ, and ($Biomass_{total}$) is the total above and below-ground plant biomass.

This approach assumes 100% mass balance via passive uptake where water and nutrients are only removed from solution via root uptake and the transpiration stream. It integrates organ-specific nutrient concentrations with their proportional contribution to total biomass for whole-plant level net nutrient replacement estimates. Thus, it provides a physiologically meaningful estimate of the whole-plants net nutrient and water removal from solution and the amount that is needed to replace it. In effect, organs with greater biomass exert more influence on the weighted value, allowing the calculation to more accurately represent the nutrient status of the entire plant rather than a single organ type.

3.2.7 Absolute Percent Deviation (APD) and Predictor Evaluation

Prediction accuracy of organ-specific and biomass-weighted nutrient input estimates was quantified using absolute percent deviation (APD). APD was calculated as:

$$APD = \frac{P - U}{U} X\ 100 \quad (4)$$

where P represents the predicted nutrient input concentration (mg L^{-1}) derived from organ-specific or biomass-weighted tissue elemental concentration scaled by plant water use efficiency (Equations 1–3), and U represents the measured nutrient uptake from solution

(mg L^{-1}), calculated as the difference between irrigation input concentration and leachate concentration at each harvest interval.

APD was calculated for each element, cultivar, predictor type (leaf, stem, root, flower, biomass-weighted including all organs [W], and biomass-weighted excluding flower tissue [WNF]), and harvest date. For each element–cultivar–harvest combination, the predictor yielding the lowest APD was identified as the optimal predictor for that interval. These harvest-resolved APD outcomes were used to evaluate temporal shifts in predictor performance across reproductive development.

For life-cycle comparisons, APD values were averaged across harvest intervals restricted to periods in which mass-balance assumptions were satisfied. The first harvest was excluded due to incomplete pairing of tissue and leachate measurements, and the final two harvests were excluded because increasing substrate nutrient accumulation violated steady-state mass-balance conditions. Mean APD across the retained interval was used to identify the most accurate predictor over the reproductive phase.

3.2.8 Statistical Analysis

Nutrient uptake from solution data for ten essential elements were analyzed using linear mixed-effects models (LMMs) to account for repeated measures across time and cultivar. Uptake values were modeled as a function of collection date (fixed within-subject factor), cultivar (fixed between-subject factor), and their interaction, with replicate treated as a random intercept to capture plant-level variance. Models were fit using the lmer function in the lme4 package. To assess robustness to outliers and leverage points—identified via Cook's distance—each model was re-estimated using robust linear mixed models (RLMMs) via rlmer from the robustlmm package. Residual diagnostics (Q–Q plots, residuals vs. leverage, and Cook's distance) were used to confirm model assumptions.

Pairwise comparisons between cultivars across time points were performed using estimated marginal means (EMMs) via the emmeans package, with Bonferroni adjustment for multiple testing. Summary plots with standard error bars (± SE) were generated using ggplot2 to visualize temporal uptake trends and cultivar separation. All statistical analyses were conducted in R version 4.3.2 (R Core Team, 2024, version 4.3.1).

3.3 Results

3.3.1 Macro/Micronutrient Uptake

Figure 1 illustrates the net nutrient removal from the container solution (net solution removal) from the irrigation solution between cultivars throughout the course of the generative phase for the major elements. First light consistently extracted more elements from the irrigation solution than CJ2 (Figure 1). Initially, both cultivars exhibited an increase in net solution removal from DFPC 0 to 60, which peaked at DFPC 20. After this point, net removal declined steadily in both cultivars for the remainder of the reproductive phase. Negative values in Figure 1 indicate net nutrient accumulation in the irrigation solution, first evident after harvest 6 (DFPC 50) and declining further at harvest 7 (DFPC 60). Net solution removal differences between cultivars, although significant, varied by element. In First Light, N shifted from 130 mg L^{-1} net removal to +109 mg L^{-1} accumulation and K from 192 mg L^{-1} net removal to +195 mg L^{-1} enrichment; in CJ2, N ranged from 90 mg L^{-1} net removal to +101 mg L^{-1} enrichment and K from 102 mg L^{-1} net removal to +195 mg L^{-1} enrichment. Phosphorus excursions were smaller (First Light: 58 to 13 mg L^{-1}; CJ2: 42 mg L^{-1} removal to +2 mg L^{-1} enrichment). Mg net removal was greater in First Light than CJ2 (37 vs. 16 mg L^{-1}). At the last two collection points, the substrate showed accumulation of the respective elements which led to negative values (accumulation).

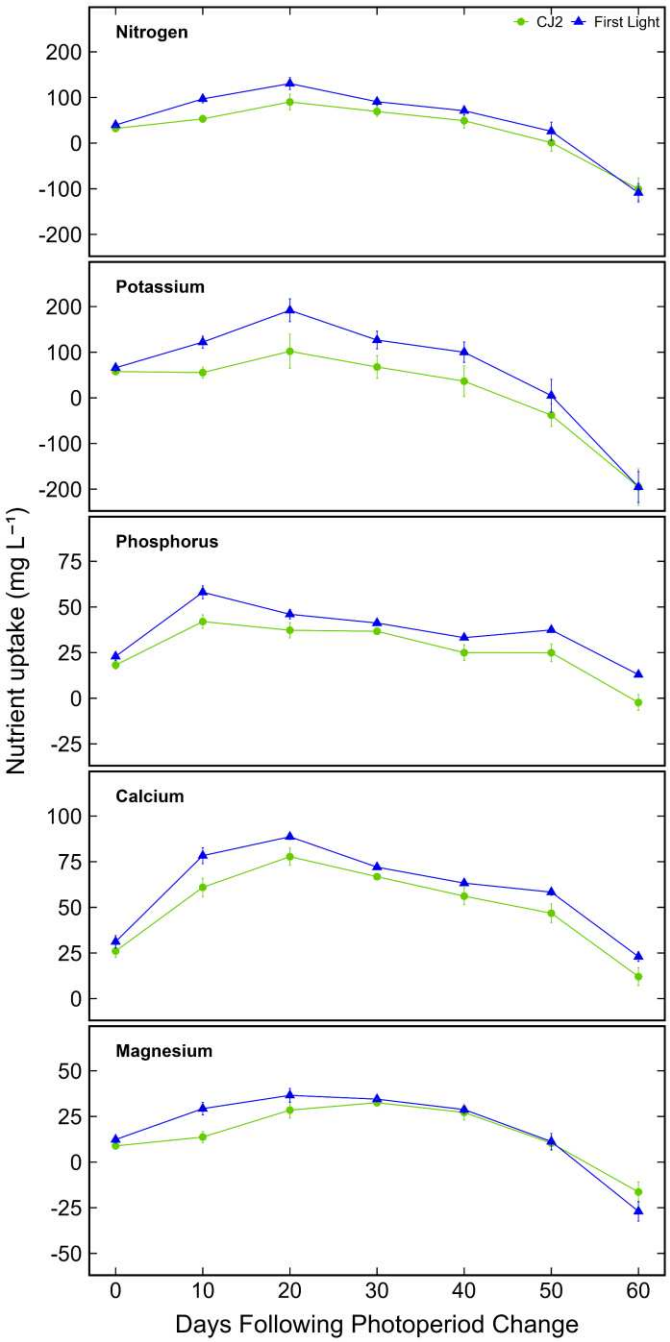

Figure 1 Uptake of nitrogen, potassium, phosphorus, calcium, and magnesium from irrigation solution (mg L^{-1}) from days following photoperiod change 0 – 60. Cultivar means for CJ2 (green solid circles) and First Light (blue solid triangles) ± SE (n = 8 per cultivar days following photoperiod change 0 – 40; n = 5 First Light and n = 4 CJ2 days following photoperiod change 50 and 60).

Across the full-time course, cultivar differences were strongest for K ($p = 0.004$), followed by Mg ($p = 0.025$), N ($p = 0.030$), and P ($p = 0.046$), whereas Ca did not exhibit a significant overall difference ($p = 0.078$). Figure 2 illustrates the nutrient solution removal from the irrigation solution between cultivars over the course of the generative phase for the minor elements. Throughout the first three leachate observation periods, First Light consistently extracted more minor elements from the nutrient solution than CJ2, and this pattern was most pronounced for Mn and B. Over the entire reproductive phase, minor element cultivar net solution removal differences were strongest for Mn ($p < 0.001$) and B ($p < 0.01$), while Fe ($p = 0.307$), Cu ($p = 0.657$), and Zn ($p = 0.460$) did not exhibit significant overall cultivar differences. Fe showed a consistent trend of greater net solution removal in First Light, but this was only supported at isolated harvest dates. B net solution removal increased from 0.035 to 0.11 mg L^{-1} in CJ2 in the beginning and from 0.04 to 0.11 mg L^{-1} in First Light while overall the highest removal was 0.12 mg L^{-1} in both cultivars before a decline in net solution removal began at DFPC 50. Zn and Cu displayed no consistent cultivar separation across the cycle. Mn diverged clearly at the 0 and 10 harvests, with CJ2 showing increased net solution removal 0.03 – 0.17 mg L^{-1} relative to earlier dates while First Light remained stable, driving the overall cultivar difference.

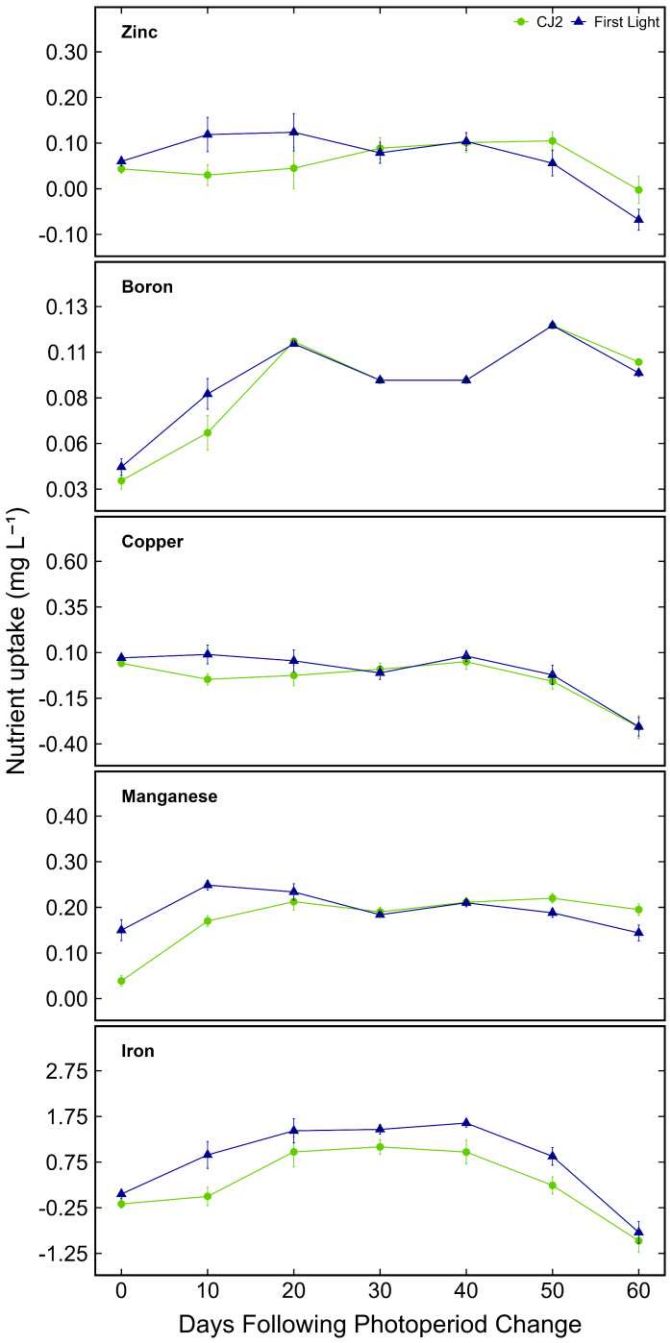

Figure 2 Uptake of boron, copper, iron, manganese, and zinc from irrigation solution (mg L^{-1}) from days following photoperiod change 0 – 60. Cultivar means for CJ2 (green solid circles) and First Light (blue solid triangles) ± SE (n = 8 per cultivar days following photoperiod change 0 – 40; n = 5 First Light and n = 4 CJ2 days following photoperiod change 50 and 60).

3.3.2 Water Use Efficiency

Overall, WUE for CJ2 was higher than First Light (Figure 3). Over the reproductive cycle, CJ2 established a peak WUE on DFPC 30 of 4.5 g L^{-1}, whereas First Light demonstrated a plateau at DFPC days 20 and 30 of 3.39 and 3.33 g L^{-1} respectively (Figure 3). Over the reproductive cycle, between cultivar WUE increased and/or decreased in unison, tracking environmental variation.

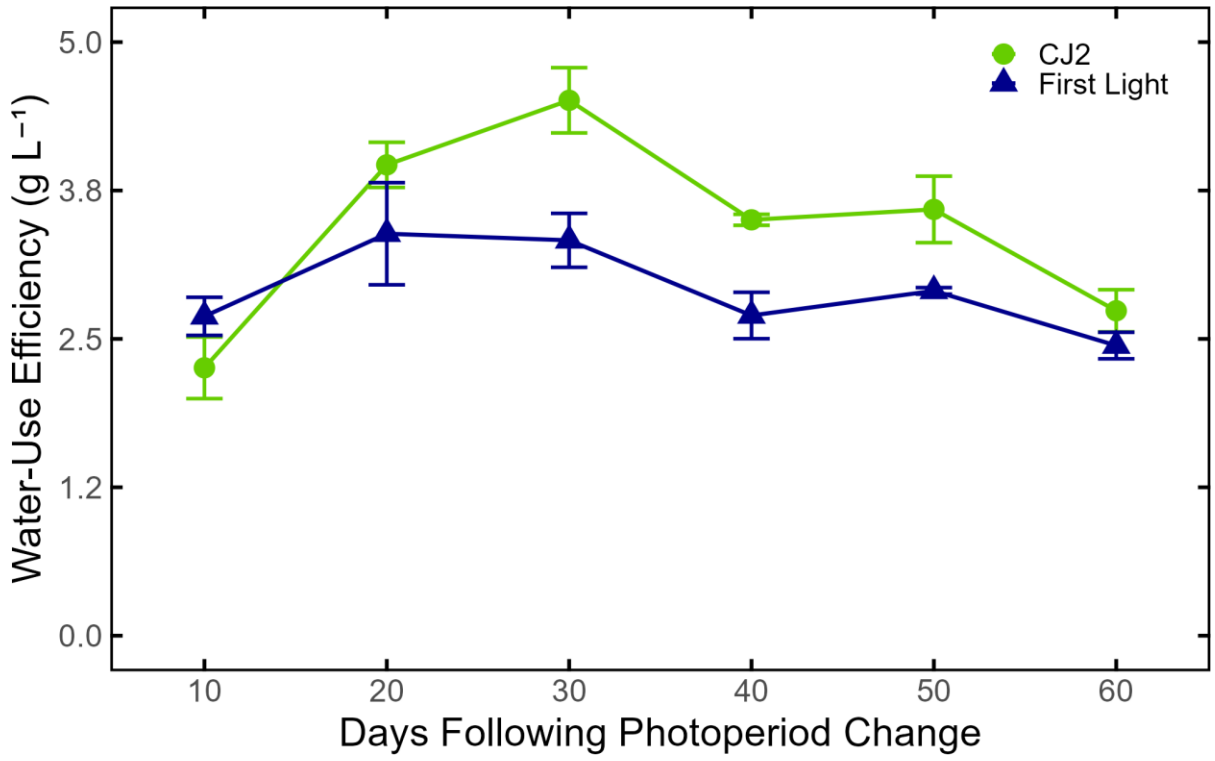

Figure 3. Water use efficiency (WUE, g L^{-1}) throughout the study (days following photoperiod change 10 – 60) for the means of two cultivars First Light (blue solid triangle) and CJ2 (green solid circle) ± SE (n = 8).

3.3.3 Macro/Micro Tissue Analysis

Figure 4 illustrates the tissue element concentrations per organ over the course of the generative phase for the major elements. Ca and Mg concentrations steadily increased in leaf tissue, whereas N declined and P and K stayed relatively constant. Similarly, P concentrations increased in CJ2 root tissue, whereas a decrease in Mg occurred in the root

tissue of both cultivars (Figure 4). K exhibited a steady decrease in stem tissue concentrations, whereas other organ K concentrations remained relatively constant. Overall, macroelement leaf tissue nutrient concentrations were within sufficient ranges throughout the generative phase (Cockson et al., 2020; Hershkowitz et al., 2025; Landis et al., 2019).

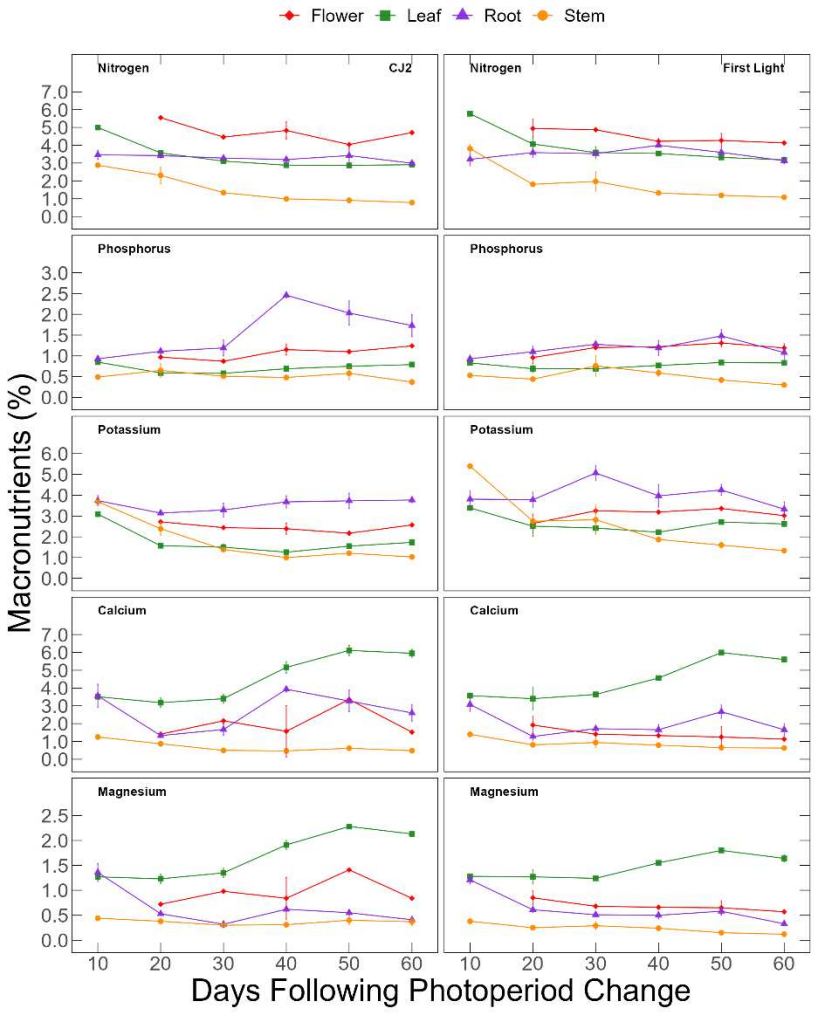

Figure 4. Tissue nutrient concentration (%) among organs for macro elements nitrogen, phosphorus, potassium, calcium, and magnesium from days following photoperiod change 0 – 60 for cultivars CJ2 and First Light. Color and symbols (leaves = green solid square; flowers = red diamond; roots = purple triangle; and stem = orange circle) represent tissue concentrations. Symbols are the means of n = 3 replicates ± SE.

Figure 5 illustrates the tissue element concentrations per organ over the course of the generative phase for the minor elements. Over the course of the reproductive phase, Cu root concentrations increased. Similarly, B leaf concentrations showed a steady increase, whereas all other organ Cu and B concentrations stayed relatively constant throughout the study (Figure 5). Initially, Fe and Mn were elevated in the root tissue but subsequently decreased to a relatively constant value thereafter. All other organ minor element tissue concentrations were relatively constant throughout the reproductive phase. Overall, minor element leaf tissue nutrient concentrations were within adequate ranges throughout the generative phase (Cockson et al., 2020; Hershkowitz et al., 2025; Landis et al., 2019).

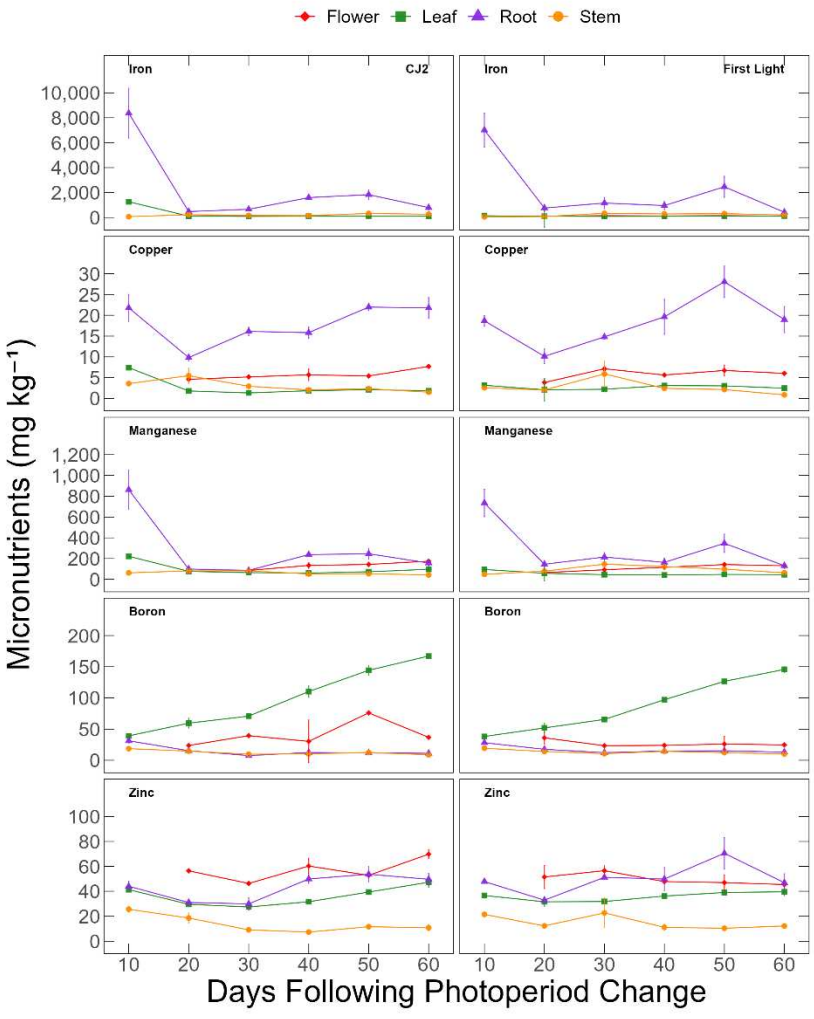

Figure 5. Tissue nutrient concentration (mg kg^{-1} dry weight (DW)) for micro elements iron, copper, manganese, boron, and zinc from days following photoperiod change 0 – 60 for cultivars CJ2 and First Light. Color and symbols (leaves = green solid square; flowers = red diamond; roots = purple triangle; and stem = orange circle) represent tissue concentrations. Symbols are the means of n = 3 replicates ± SE.

3.4 Predicted Net Solution Removal by Organ

3.4.1 Macronutrients

Figure 6 shows the cultivar difference for predicted nutrient replenishment input concentrations for macroelements N, P, K, Ca and Mg on an organ specific basis as well as element net solution removal from solution. The best predictors per element were determined by absolute percent deviation (APD). Predicted solution replenishment concentrations for N calculated from leaf, flower, or root tissue concentrations overestimated uptake from solution in CJ2. The predictions using stem tissue concentrations were the best predictors of N net solution removal from solution in all but the last two collection intervals, where on three harvests the estimation using stem tissue overestimated N by 7.52 mg L^{-1} (DFPC 20) and underestimated 8.94 mg L^{-1} (DFPC 30) and 14.24 mg L^{-1} (DFPC 40). Initially, stem tissue was again the best predictor of First Light N net solution removal, but after the initial collection interval, stem tissue concentrations underestimated First Light net solution removal from solution, whereas leaf, root, and flower tissue concentrations mostly overestimated N net solution removal (Figure 6). Over the course of the generative phase, First Light N solution net solution removal was best predicted with root tissue concentration, with an APD of 2.32%. Regardless of cultivar, P net solution removal was underestimated when leaf or stem tissue concentrations were used to derive replenishment concentrations. For CJ2, root tissue overestimated P removal, whereas flower tissue concentrations best represented P net solution removal in First Light (Figure 6).

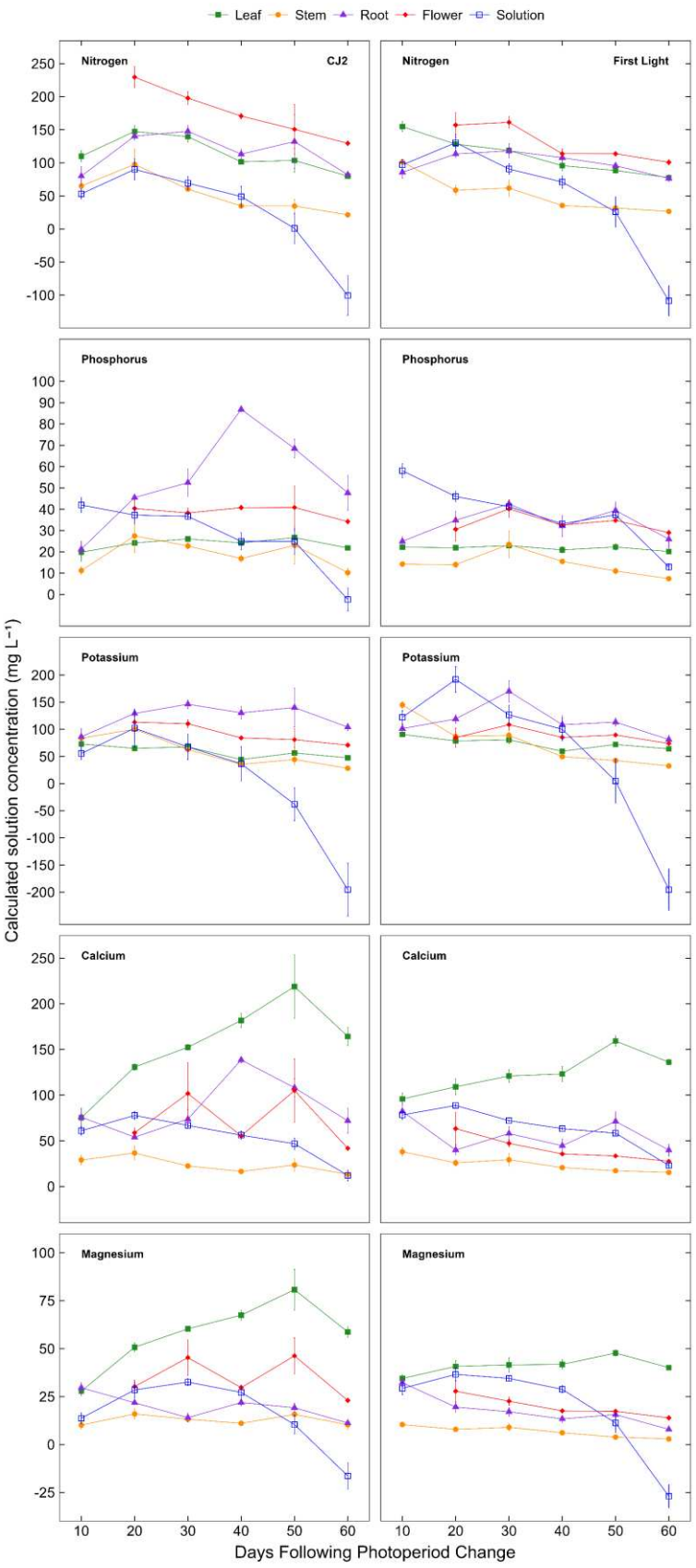
Leaf
Stem
Root
Flower
Solution
Nitrogen
CJ2
Nitrogen
First Light
Phosphorus
Phosphorus
Potassium
Potassium
Calcium
Calcium
Magnesium
Magnesium
Calculated solution concentration (mg L⁻¹)
Days Following Photoperiod Change

Figure 6 The organ specific calculated nutrient solution input concentrations for nitrogen, phosphorus, potassium, calcium, and magnesium. Each organ per cultivar, CJ2 (left panels) and First Light (right panels) was compared to the solution nutrient uptake (input concentration – leachate solution concentration). Green lines and solid squares illustrate leaf estimates; orange lines and solid circles illustrate stem estimates; purple lines and solid triangles illustrate roots estimates; red lines and solid diamonds illustrate flowers estimates; blue lines and open squares illustrate element uptake from solution from days following photoperiod change 10 – 60. Predicted values were calculated on an organ basis using the biomass and water use efficiency observations following Langenfeld et al. (2022) equation 1. Symbols are the means of n = 3 replicates ± SE.

Flowers were the best predictors for CJ2 P net solution removal, having an APD of 10.42%. Root and flower organ nutrient concentration estimates for K overpredicted net solution removal in CJ2. Underestimates of K net solution removal were prevalent in First Light for all organ estimates except the roots at harvest 4 and 5 (DFPC 30 and 40). In CJ2 the best predictor of K net solution removal was stem tissue with an absolute deviation of 9.66% and in First Light roots were the best predictor with an APD of 14.53%. Ca showed an increase in over prediction estimates using leaf tissue concentrations over time. The Ca overestimation was more prevalent in CJ2 but occurred in First Light as well. Stem tissue Ca concentrations consistently underestimated Ca net solution removal from solution in both cultivars. Overall, root and flower tissue concentrations were better predictors of Ca net solution removal from solution than leaves or stems, however, neither consistently represented Ca net solution removal from solution throughout the study. Mg net solution removal from solution was consistently overestimated with leaf tissue concentrations, whereas stem tissue consistently underestimated Mg net solution removal. Prior to the decrease in Mg net solution removal at DFPC 50, the flower organ Mg concentrations were the best predictors of magnesium net solution removal from solution. Other than the initial measurement on DFPC 10, root tissue underestimated Mg net solution removal in both cultivars until Mg net solution removal from solution decreased after DFPC 40.

3.4.2 Micronutrients

Figure 7 shows the cultivar net solution removal differences in micronutrients Fe, Cu, B, Mn and Zn. Other than B, the micronutrient solution replenishment predictions demonstrated a more consistent prediction over the course of the reproductive cycle as compared to the macroelement predictions. Regardless of organ, Fe concentration replenishment predictions were close to the net solution removal value with only small under estimation. One exception was root tissue; which over predicted at all collection intervals for both cultivars. The organ tissue that best estimated Fe removal from solution in CJ2 were leaves with an APD of 1.62%. CJ2 Cu net solution replenishment estimates were often overestimated; regardless of organ tissue Cu concentration. Alternatively, First Light organ concentrations for Cu tended to underpredict, except for DFPC 30 where overpredictions were observed at 0.06 mg L^{-1}. The predictor in First Light to best forecast Cu net solution removal was roots with an APD of 6.08%. Alternatively, CJ2 Cu replenishment predictions from stem concentrations were 0.0075 mg L^{-1} where actual net solution removal values collected were 0.0538 mg L^{-1} taken from solution. B stem tissue concentrations consistently overpredicted replenishment in both cultivars as B stem tissue concentrations increased over the course of the generative phase, the deviation between the net solution removal from solution versus the predicted replenishment deteriorated further. For B, predictions derived from leaf and root tissue concentrations consistently underestimated net solution removal from solution in both cultivars where the leaves and roots underpredicted by 0.05 ppm and 0.04 ppm. Leaves exhibited an underprediction of 0.05 mg L^{-1} while roots values were 0.04 mg L^{-1} below the actual solution net solution removal. Root tissue Mn and Zn concentrations primarily over predicted CJ2 and First Light net solution removal from solution. The same result occurred for flower tissue for Zn predictions in First Light. In general, all organ tissue element concentrations for Mn and Zn overpredicted net solution removal from solution. The best predictor for Mn net solution removal for both cultivars were leaves, having an APD of 15.33% for CJ2 and 22.63% for

First Light. Zn had a mostly unwavering net solution removal from solution until the last collection on DFPC 60. Individual organ predictions in First Light were dominated by underestimation where in CJ2 overestimation prevailed.

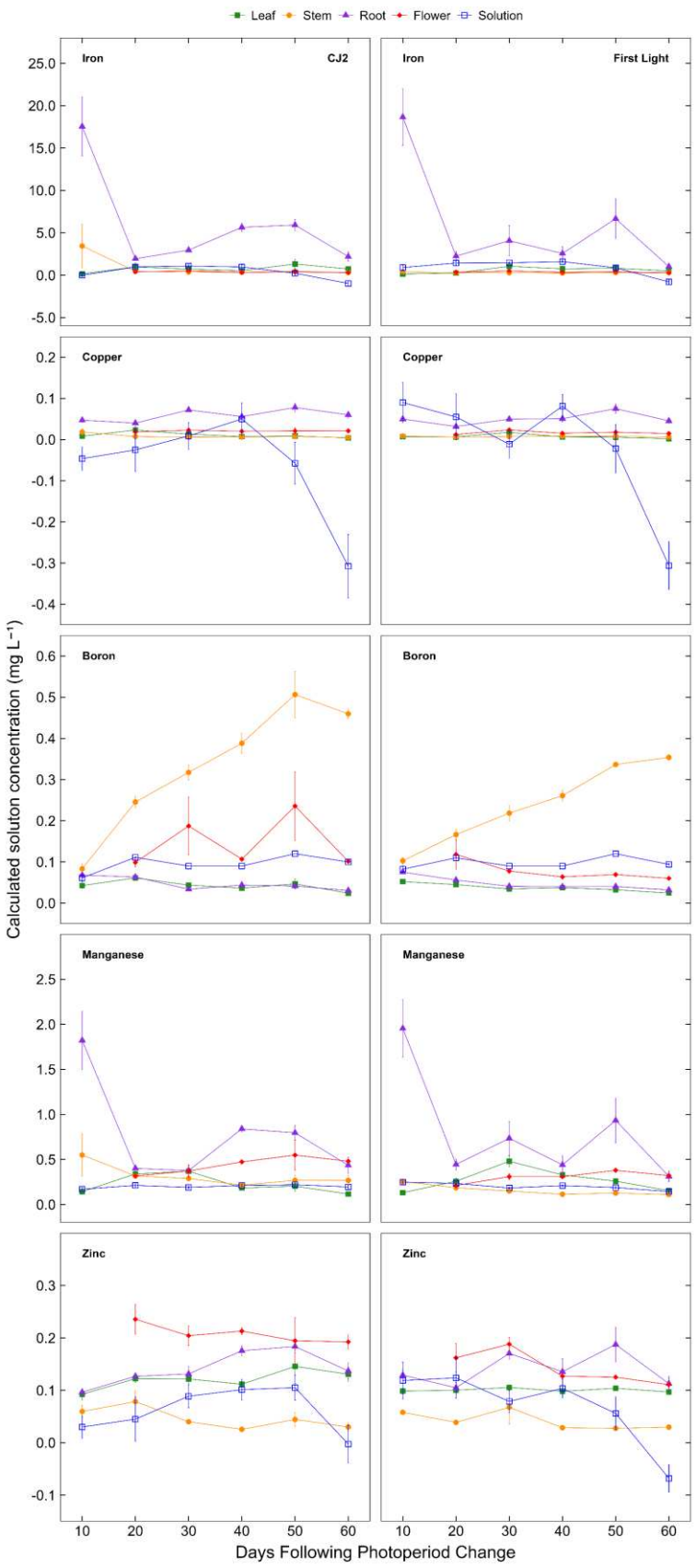
Leaf
Stem
Root
Flower
Solution
Iron
CJ2
Iron
First Light
Copper
Copper
Boron
Boron
Manganese
Manganese
Zinc
Zinc
Calculated soluton concentration (mg L⁻¹)
Days Following Photoperiod Change

Figure 7. The organ specific calculated nutrient solution input concentration for iron, copper, boron, manganese, and zinc. Each organ per cultivar, CJ2 (left panels) and First Light (right panels), was compared to the solution nutrient uptake (input concentration – leachate solution concentration). Green lines and solid squares illustrate leaf estimates; orange lines and solid circles illustrate stem estimates; purple lines and solid triangles illustrate roots; red lines and solid diamonds illustrate flowers; blue lines and open squares illustrate element uptake from solution from days following photoperiod change 10 – 60. Predicted values were calculated on an organ basis using the biomass and water use efficiency observations following Langenfeld et al. (2022) equation 1. Symbols are the means of n = 3 replicates ± SE.

3.5 Weighted Organ Predictions

Figures 8 and 9 compare organ biomass-weighted mean replenishment predictors for macroelements (Figure 8) and microelements (Figure 9) against measured nutrient net solution removal from solution. Biomass-weighted means were calculated using all organs (W) and with flower tissue excluded (WNF) to avoid bias from potential luxury accumulation in reproductive tissues. Across elements and cultivars, the performance of biomass-weighted means relative to the best single-organ predictors was element- and cultivar-specific.

For cultivar CJ2, WNF provided the lowest absolute percent deviation (APD) for N, Ca, Mg, B, and Zn, with APDs of 7.33%, 0.92%, 5.62%, 12.39%, and 7.15%, respectively. In these cases, WNF either matched or improved upon the closest single-organ replenishment predictor, indicating that integrating vegetative organ biomass reduced organ-specific bias and better captured whole-plant net solution removal dynamics. For example, while leaf or root tissues individually over- or under-predicted replenishment for several elements, the WNF approach consistently reduced prediction error by balancing contrasting organ signals. Notably, inclusion of flower tissue (W) did not improve prediction accuracy for any element in CJ2, reinforcing the potential for reproductive tissues to distort biomass-weighted estimates during flowering.

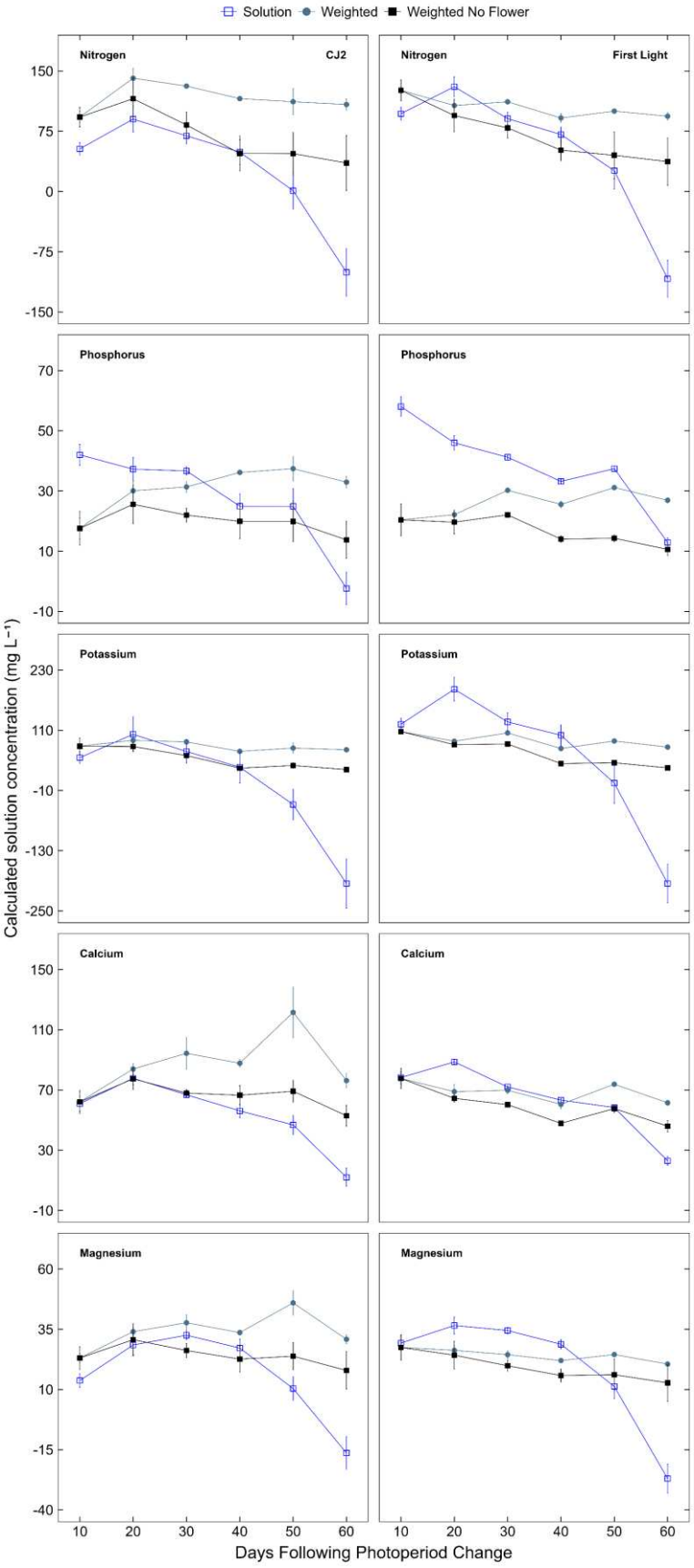
Solution
Weighted
Weighted No Flower
Nitrogen
CJ2
Nitrogen
First Light
Phosphorus
Phosphorus
Potassium
Potassium
Calcium
Calcium
Magnesium
Magnesium
Calculated solution concentration (mg L⁻¹)
Days Following Photoperiod Change

Figure 8. Calculated nutrient solution input concentrations for nitrogen, phosphorus, potassium, calcium, and magnesium expressed on an organ biomass-weighted mean with (W) and without (WNF) flower tissue included in the organ biomass-weighted mean. All organ W values (teal solid circle) along with WNF (black solid squares) per cultivar, CJ2 (left panels) and First Light (right panels), compared to the solution nutrient uptake (open blue squares; input concentration – leachate solution concentration) from days following photoperiod change 10 – 60. Predicted values were calculated using the biomass and water use efficiency observations following Langenfeld et al. (2022), equation 1. Symbols are the means of n = 3 replicates ± SE.

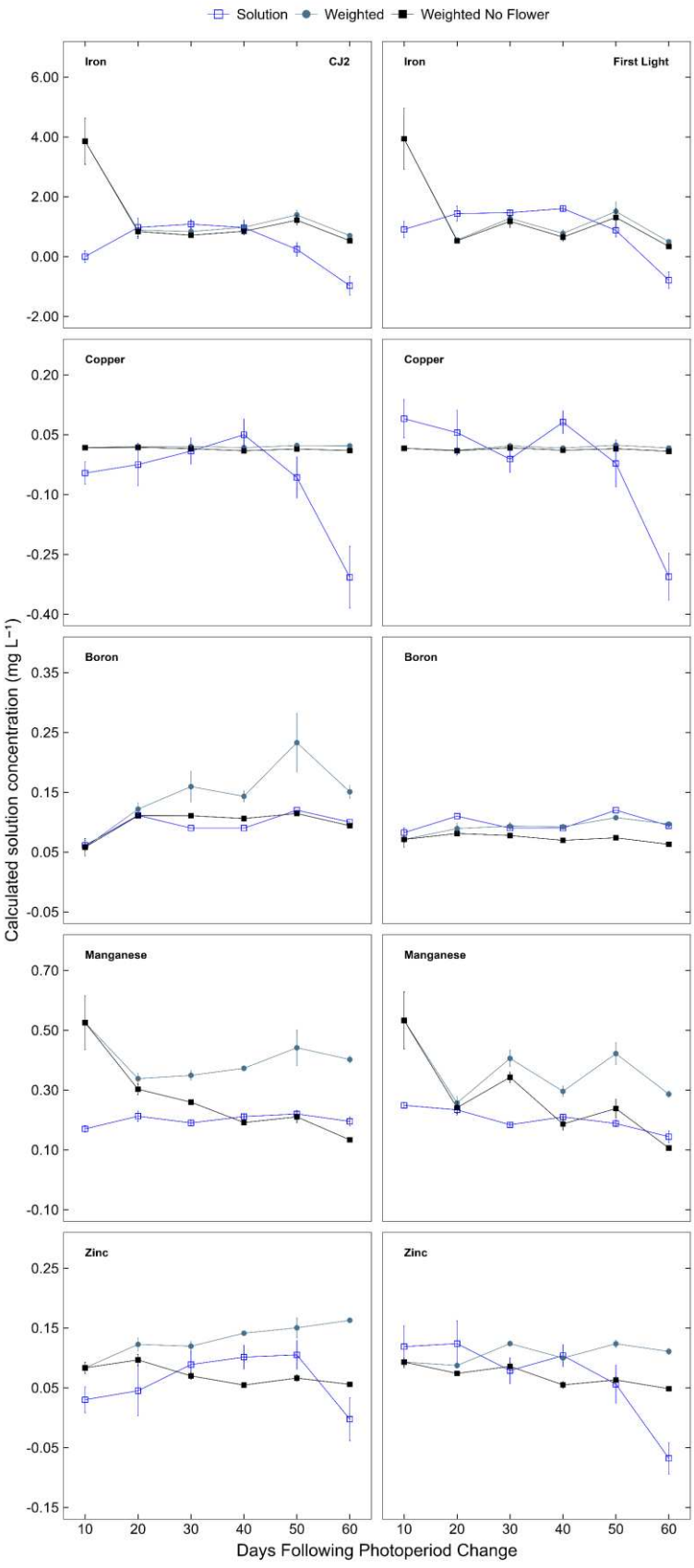
Solution
Weighted
Weighted No Flower
Iron
CJ2
Iron
First Light
Copper
Copper
Boron
Boron
Manganese
Manganese
Zinc
Zinc
Calculated solution concentration (mg L⁻¹)
Days Following Photoperiod Change

Figure 9. The calculated nutrient solution input concentrations for iron, copper, boron, manganese, and zinc expressed on an organ biomass-weighted mean with (W) and without (WNF) flower tissue included in the organ biomass-weighted mean. All organ W values (teal solid circle) along with WNF (black solid squares) per cultivar, CJ2 (left panels) and First Light (right panels), compared to the solution nutrient uptake (open blue squares; input concentration – leachate solution concentration) from days following photoperiod change 10 – 60. Organ biomass-weighted mean predicted values were calculated using the biomass and water use efficiency observations method following Langenfeld et al. (2022), equation 1. Symbols are the means of n = 3 replicates ± SE.

In First Light, the relative benefit of biomass-weighted means was more variable. WNF was the best predictor for Fe replenishment (APD = 2.28%), outperforming individual organs and suggesting improved integration of vegetative demand for this element. In contrast, Ca, Mg, B, and Zn replenishment was best predicted by W, with APDs of 9.11%, 25.0%, 1.56%, and 0.06%, respectively. For these elements, inclusion of flower biomass improved prediction accuracy relative to the best single-organ predictors, indicating that reproductive tissues contributed meaningfully to whole-plant elemental removal in First Light. However, for Mg in particular, the relatively high APD suggests limited improvement over single-organ predictors, highlighting that biomass weighting does not universally enhance predictive performance.

Overall, these results show that organ biomass-weighted means can improve alignment with solution-based removal compared to single-organ predictors, but the magnitude and direction of improvement depend on both cultivar and element. Excluding flower tissue generally improved prediction accuracy in CJ2, whereas inclusion of flowers benefited prediction for several elements in First Light, underscoring cultivar-specific differences in nutrient partitioning during the reproductive phase.

3.6 Temporal Stability of Optimum Predictors Across Reproductive Development

When prediction accuracy was evaluated on a harvest-by-harvest basis, the identity of the optimal replenishment predictor varied across developmental time. No single organ consistently minimized absolute percent deviation (APD) across all harvests. Single-organ predictors, particularly stem, frequently produced the lowest APD at individual time points

but exhibited marked temporal variability (Figure 10). In contrast, the WNF maintained comparatively stable performance across harvests and did not exhibit the pronounced stage-specific shifts observed in single-organ predictors. Although the WNF replenishment predictor was not the most frequent best predictor at every harvest, it minimized cumulative error more consistently across developmental transitions, indicating greater temporal robustness for life-cycle nutrient replenishment estimation (Figure 10). These results suggest that temporally stable composite predictors may be more suitable for mass-balance–based fertigation replenishment modeling than predictors that are intermittently optimal but developmentally sensitive.

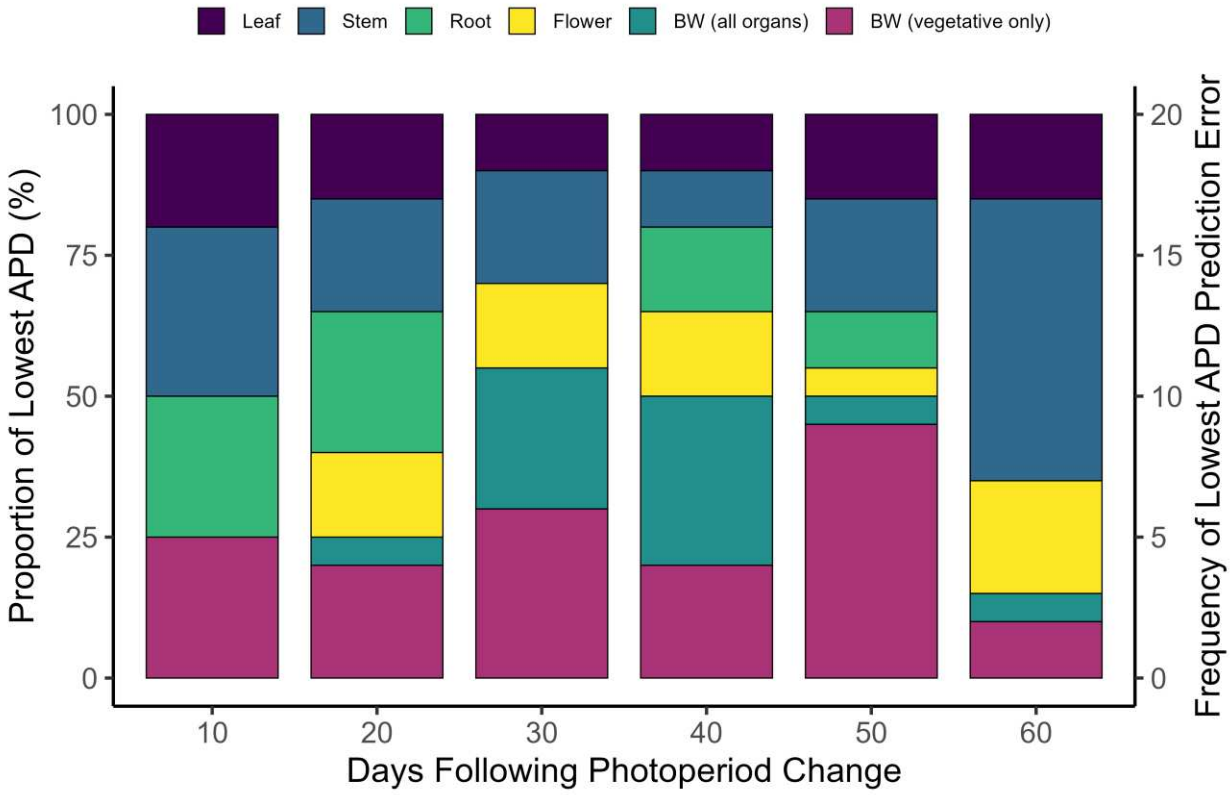

Figure 10. Optimal predictor frequency by harvest date based on absolute percent deviation (APD) calculated between predicted nutrient input and measured solution uptake. Stacked bars represent the number of element × cultivar combinations for which each predictor produced the lowest APD at a given harvest. Predictor identity varied across developmental stages, with no single organ consistently minimizing error through time. BW = biomass-weighted composite predictor. All organs = leaf + stem + root + inflorescence; vegetative only = leaf + stem + root.

3.7 Optimal Replenishment Prediction Method

To operationalize fertigation decisions from element-specific time courses, we reduced each candidate's replenishment predictor, single-organ concentrations and biomass-weighted means, to a mean over the interval where net nutrient solution removal provided a defensible benchmark. In Supplementary Figures 1 and 2, each point represents the mean predicted replenishment for a given predictor–element combination, plotted relative to the mean measured net solution removal. The predictor with the lowest APD for each element–cultivar pair is plotted to illustrate systematic bias: displacement above the net solution removal marker indicates over-prediction, whereas displacement below indicates under-prediction (Supplementary Figures 1 and 2).

Data aggregation was intentional to emphasize the most defensible growth intervals. The first harvest was excluded because tissue and leachate data were not adequately paired, and DFPC 50 and 60 were omitted due to increasing substrate nutrient concentrations that deviated from mass-balance estimates. The retained interval therefore reflects conditions under which replenishment-based comparisons are most reliable. Within these figures, an organ-biomass weighted predictor was the best for predicting element removal from solution in the majority of macroelement comparisons, suggesting that relative organ biomass averaging captured net solution removal better than single-organ concentrations. This also occurred in the microelement predictors where five out of ten comparisons illustrate that the best predictor was a biomass weighted value that excluded the flower organ (Supplementary Figure 2). Aggregated predictor performance was visualized to facilitate comparison of relative deviation magnitudes across elements and cultivars; these reproductive cycle APD summaries are presented in Supplementary Figure 1 and 2.

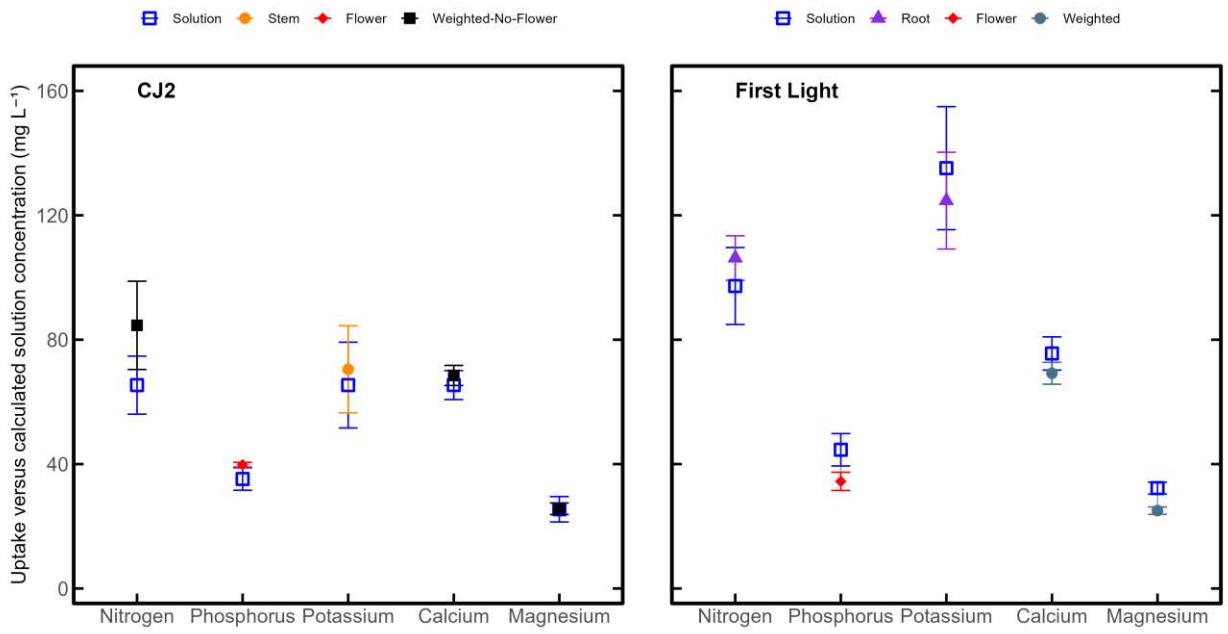

Supplementary Figure 1. Plant nutrition for cultivars CJ2 (left panel) and First Light (right panel) show element uptake (mg L^{-1}) for macro elements nitrogen, phosphorus, potassium, calcium and magnesium. Weighted value (teal solid circle); weighted no flower (black solid square); stem (orange solid circle); flower (red solid diamond); root (purple solid triangle) and solution nutrient uptake (input concentration – leachate nutrient concentration, blue open square) mean of all harvest intervals ± SE (n = 4).

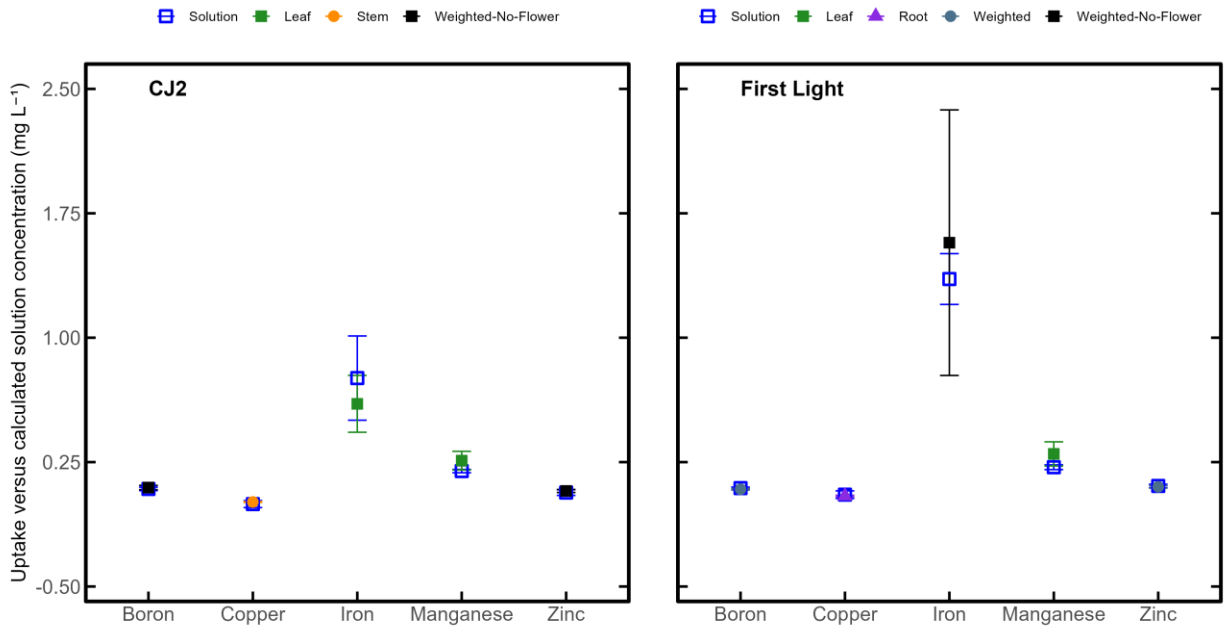

Supplementary Figure 2. Plant nutrition for cultivars CJ2 (Left) and First Light (Right) show element uptake (mg L^{-1}) for micro elements boron, copper, iron, manganese, and zinc. Weighted value (teal solid circle); weighted no flower (black solid square); leaf (green solid square); stem (orange solid circle); root (purple solid triangle) and solution nutrient

uptake (input concentration – leachate nutrient concentration, blue open square) mean of all harvest intervals ± SE (n = 4).

3.8 Discussion

3.8.1 Transpiration-Driven Mass Balance During the Reproductive Phase

The present findings extend vegetative-phase mass-balance principles into the reproductive phase of *C. sativa*, demonstrating that net solution removal from solution remains tightly coupled to transpiration-driven fluxes rather than fixed solution concentrations (Langenfeld et al., 2022; Langenfeld & Bugbee, 2024; Powell & Bauerle, 2026). Across both cultivars, nutrient extraction from the irrigation solution increased following floral initiation, peaked mid-flowering, and declined steadily thereafter (Figures 1 and 2), mirroring concurrent changes in WUE (Figure 3). This temporal coupling confirms that nutrient demand during flowering is dynamic and coupled to whole-plant water flux.

Consistent with prior zero-discharge and closed-loop studies, nutrient removal from solution tracked plant uptake rather than remaining proportional to imposed fertigation setpoints (Langenfeld et al., 2022; Langenfeld & Bugbee, 2024). Declining removal later in the generative phase coincided with reduced transpiration and WUE, underscoring the biophysical basis of transpiration-scaled nutrient delivery. Together, these results highlight a fundamental limitation of static EC setpoints during reproductive development, when nutrient demand decouples from imposed fertigation targets as transpiration declines and inflorescences mature.

3.8.2 Organ Divergence and Phenology-Driven Partitioning

Organ-level tissue analysis revealed pronounced divergence in elemental concentrations across flowering. Leaf Ca and Mg concentrations increased steadily during reproduction, while leaf N declined, consistent with reduced vegetative expansion and altered source–sink relations (Massuela et al., 2023; Saloner & Bernstein, 2023). These

shifts intensified as phenology advanced, undermining the assumption that single-organ elemental concentrations reliably reflect whole-plant nutrient demand throughout flowering.

Although Mg net solution removal from solution declined over time (Figure 1), Mg concentrations in leaf tissue continued to increase, particularly in CJ2. Because tissue harvests were conducted on pooled leaf biomass rather than selectively sampling upper, recently expanded leaves, this pattern indicates progressive internal redistribution of Mg from stems and roots to leaves rather than sustained external acquisition. Magnesium is phloem mobile, and its remobilization from structural tissues to metabolically active leaves under declining growth and transpiration aligns with established models of nutrient recycling during reproductive development and senescence (H. Marschner, 2012). Correspondingly, decreasing Mg pools in stems and roots support the interpretation that internal translocation governed leaf Mg accumulation late in flowering.

Interestingly, Ca, despite being classically regarded as phloem immobile, exhibited a qualitatively similar temporal trajectory in leaf tissue accumulation. While absolute Ca concentrations differed from Mg, the shapes of the uptake and tissue accumulation curves were similar (Figure 4). This convergence likely reflects shared biophysical constraints imposed by declining transpiration and growth rates during late flowering, which limit xylem delivery to expanding tissues while concentrating Ca in persistent leaves as biomass accumulation slows (Hawkesford et al., 2012). Thus, parallel Ca and Mg trends do not imply shared mobility mechanisms, but rather a common response to phenology-driven reductions in water flux.

Collectively, these organ-specific reproductive stage trajectories demonstrate that internal redistribution and phenological context influence tissue nutrient profiles during flowering. Reliance on single-organ diagnostics during the reproductive phase therefore risks systematic misrepresentation of whole-plant nutrient demand, with both the direction and magnitude of bias dependent on element mobility and developmental stage. Similar patterns of organ divergence have been reported in flowering *C. sativa* and other

reproductive crops, where nutrient partitioning shifts rapidly with sink dominance (Saloner & Bernstein, 2023; Westmoreland & Bugbee, 2022).

3.8.3 Biomass-Weighted Nutrient Replacement Predictors and Genotype-Specific Responses

Integrating organ nutrient concentrations using biomass-weighted means generally provided a more accurate representation of whole-plant nutrient demand than single-organ replacement estimates across most elements and time points (Figures 8 and 9). Biomass-weighted means excluding flower tissue in general aligned consistently with measured solution uptake for N, Ca, Mg, B, and Zn in CJ2, and for Fe in First Light. This outcome supports exclusion of reproductive tissues when estimating nutrient replenishment amounts, given recent evidence for *C. sativa* luxury accumulation and nutrient storage in flowers without proportional yield or quality benefits (Hershkowitz et al., 2025; Westmoreland & Bugbee, 2022).

The correspondence between declining solution removal of N and K and decreasing predicted replenishment concentrations further validates the transpiration-driven nutrient replenishment mass-balance framework. As flowering progressed and plants approached senescence, reductions in transpiration and WUE coincided with diminished drawdown from solution of these highly mobile elements, consistent with declining physiological age organ metabolic activity in *C. sativa* (Bauerle et al., 2020). Predicted replacement inputs decreased accordingly, confirming that the framework responds to phenology-driven reductions in nutrient demand. However, we note that the mass-balance nutrient replenishment framework consistently over estimated replenishment rates during this phase of the regenerative cycle.

In contrast, Mg displayed an opposing pattern in CJ2, where predicted replenishment input concentrations increased despite declining uptake from solution. This apparent discrepancy could be a result of internal redistribution where increasing leaf Mg concentrations reflect translocation from stems and roots rather than increased root

acquisition. When predicted replenishment rates are derived from biomass-weighted tissue stoichiometry scaled by whole-plant water use, the framework captures changes in internal elemental allocation. Thus, increasing predicted Mg replenishment amounts do not imply increased Mg net removal from the solution, but rather could reflect shifting internal pools under declining transpiration.

Some genotype-specific differences were evident throughout the reproductive phase. First Light removed greater quantities of nutrients early in flowering, whereas CJ2 maintained higher WUE, producing distinct mass-balance replenishment amounts under identical fertigation regimes. These differences are consistent with genotype-dependent coupling between transpiration, nutrient flux, and canopy function previously reported in hemp and cannabis systems (Baumgardner et al., 2021; Powell & Bauerle, 2026; Saloner et al., 2019; Tang et al., 2018). Although individual organs occasionally approximated uptake better than WNF for some specific elements, these relationships were transient and element specific. Overall, biomass-weighted predictors provided the most consistent and physiologically grounded means to estimate whole-plant nutrient replenishment amounts during the flowering phase in *C. sativa*.

3.8.4 Temporal Robustness and Model Applicability

While mean APD comparisons identified element- and cultivar-specific optimal predictors, the harvest-resolved analysis revealed that predictor identity was not constant across reproductive development. Single-organ predictors, particularly stems and roots, occasionally minimized prediction error but exhibited pronounced temporal variability. This instability in one particular organ or biomass-weighted input tissue element concentration could reflect developmental shifts in organ function, biomass allocation, and internal nutrient redistribution, which alter the relationship between local tissue concentration and whole-plant nutrient demand during reproductive development (Massuela et al., 2023; Saloner & Bernstein, 2023). Consequently, tissue element concentration predictors that

perform well at a single developmental stage may systematically misrepresent demand when applied across the entire reproductive cycle.

In contrast, biomass-weighted composite predictors, especially those that excluded reproductive tissue, demonstrated greater temporal stability, which comparatively resulted in lower error across the reproductive phase (Supplemental Figures 1 and 2). The exclusion of reproductive tissue likely reduced over estimation that could result from luxury accumulation and transient nutrient storage that does not scale proportionally with transpiration-driven uptake (Hershkowitz et al., 2025; Westmoreland & Bugbee, 2022). From a fertigation perspective, temporal robustness is more operationally meaningful than intermittent optimality. Nutrient replacement decisions occur continuously rather than at individual developmental stages, particularly in controlled-environment production systems where fertigation schedules can alter throughout the production cycle (Langenfeld et al., 2022; Sperling et al., 2020). A nutrient replacement predictor that minimizes cumulative error across time therefore provides a more reliable estimate for dynamic nutrient management throughout a crop's life cycle.

These findings reinforce that reproductive-phase nutrition cannot be inferred from single-organ diagnostics or static tissue element concentration targets. Instead, accurate nutrient replacement requires integration of biomass partitioning, phenological stage, and transpiration-scaled flux (Langenfeld et al., 2022; Langenfeld & Bugbee, 2024). The temporal instability of organ-specific predictors further underscores why fixed EC or input concentration setpoints fail during flowering: as internal nutrient allocation and water flux decline, the relationship between tissue concentration and net nutrient removal from solution becomes increasingly nonlinear (Massuela et al., 2023; Saloner & Bernstein, 2023). Organ biomass-weighted mass-balance approaches mitigate this individual organ estimate instability by integrating organ-level divergence across the whole plant into a single physiologically grounded predictor of whole-plant demand (Powell & Bauerle, 2026).

3.8.5 Temporal Dynamics and the Failure of Static Nutrient Input Setpoints

The temporal variation of net nutrient removal from solution across the reproductive phase in *C. sativa* illustrates why static fertigation setpoints underperform during *C. sativa* reproductive development. Early flower development coincided with strong inflorescence sink activity, elevated transpiration, and pronounced solution drawdown, whereas late-stage flowering was characterized by declining net solution removal despite continued nutrient availability (Figures 1 and 2). This downturn tracked reductions in transpiration and altered organ nutrient allocation, reinforcing the need for stage-specific adjustments in nutrient delivery (Langenfeld et al., 2022; Saloner & Bernstein, 2023).

Importantly, declining net solution removal from solution does not imply uniform depletion of tissue nutrient pools. For mobile elements such as N and K, reduced nutrient solution drawdown was accompanied by declining tissue concentrations, consistent with diminished ontogenetic organ metabolic activity and progressive nutrient remobilization as plants approached senescence (Bauerle et al., 2020). In these cases, decreasing predicted replacement concentrations aligned with both solution- and tissue-based indicators of nutrient concentration.

By contrast, Mg exhibited a temporal decoupling between net solution removal and tissue accumulation, particularly in CJ2. Although Mg removal from solution declined, leaf Mg concentrations continued to increase due to internal redistribution from stems and roots. Under these conditions, static fertigation setpoints would misinterpret continued tissue accumulation as sustained tissue external demand, whereas the mass-balance framework, when paired with organ-level tissue analysis, correctly distinguishes internal translocation from root uptake.

Taken together, organ-level nutrient concentration divergence, plant internal nutrient redistribution, and declining transpiration across the reproductive phase demonstrate that reproductive-phase nutrient requirements in *C. sativa* is governed by dynamic, organ metabolic activity and water flux rather than static nutrient input solution concentrations,

requiring fertigation strategies that integrate phenology, biomass partitioning, and transpiration-scaled mass balance to accurately reflect whole-plant nutrient replenishment.

3.8.6 Implications for Fertigation Practice and Policy

Across controlled-environment agriculture (CEA), evidence increasingly supports transpiration-coupled, mass-balance fertigation strategies over fixed nutrient recipes (Langenfeld et al., 2022; Powell & Bauerle, 2026; Sperling et al., 2020). In greenhouse and CEA systems, nutrient replenishment inputs scaled to water loss consistently reduce discharge and improve nutrient use efficiency (Blok et al., 2023; Li et al., 2024; Westmoreland & Bugbee, 2022). Dynamic fertigation studies in tomato further demonstrate large discrepancies between balance-based uptake estimates and dry-matter accounting, revealing system-level sinks that static EC management fails to detect (Cedeño et al., 2023, 2024). Despite decades of fertigation research in horticultural crops, most nutrient solution input concentration management frameworks continue to rely on static solution concentrations or EC targets that cannot resolve phenology-driven shifts in transpiration, internal nutrient redistribution, or the decoupling of tissue accumulation from external uptake observed during reproductive development.

In *C. sativa*, fertigation strategy reshapes the ionome along with downstream biomass and cannabinoid outcomes, emphasizing that nutrient flux, not solution concentration alone, governs crop performance (Velechovský et al., 2024). Operationally, nutrient mass-balance frameworks can reduce fertilizer loss, minimize wastewater handling, and facilitate compliance with emerging regulatory constraints that prioritize measurement-based nutrient stewardship (Ontario Ministry of the Environment, Conservation and Parks (MECP), 2022). Because EC integrates all ions into a single signal and obscures element-specific behavior, such as K-induced suppression of Ca and Mg uptake or redistribution-driven tissue accumulation, flux-based fertigation provides a more biophysical and mass conservation defensible basis for specifying elemental resupply per unit transpired water

(Bugbee, 2004; Langenfeld et al., 2022; Langenfeld & Bugbee, 2024; Powell & Bauerle, 2026; Sperling et al., 2020).

3.9 Conclusion

This study quantified net nutrient removal from solution, organ-level and biomass-weighted elemental composition, and water use across the reproductive phase of *C. sativa*, demonstrating that net nutrient removal from solution declines with reduced transpiration late in the flowering stage. Organ nutrient concentrations diverged as phenology advanced: leaves accumulated Ca and Mg despite declining net nutrient removal from solution, while N declined; roots and stems diverged for K, consistent with *C. sativa* reproductive sink dominance and internal nutrient remobilization (Saloner & Bernstein, 2023).

Biomass-weighted means of non-reproductive organs most accurately tracked solution removal over time, with element, organ and cultivar-specific exceptions (e.g., N approximated by stems in CJ2 and roots in First Light). Cultivar contrasts were observed in this study, however, this variation was marginal: First Light removed more nutrients early in flowering, whereas CJ2 maintained higher WUE, indicating that replenishment strategies may be genotype specific. The most accurate predictor shifted with phenology, reinforcing that static nutrient proxies are insufficient during flowering and that fertigation should at least respond to observed solution drawdown rather than maintain fixed input targets (Powell & Bauerle, 2026; Westmoreland & Bugbee, 2022).

Collectively, these results support a transpiration-scaled, nutrient and WUE mass-balance framework for reproductive-phase fertigation, aligning with critiques of EC-centric control and advancing contemporary zero-discharge nutrient management strategies (Langenfeld et al., 2022; Langenfeld & Bugbee, 2024).

References

Ahmadi, F., Kallinger, D., Starzinger, A., & Lackner, M. (2024). Hemp (*Cannabis salvia* L.) Cultivation: Chemical Fertilizers or Organic Technologies, a Comprehensive Review. *Nitrogen*, *5*(3), 624–654. https://doi.org/10.3390/nitrogen5030042

Ahmed, M., Aslam, M. A., Fayyaz-ul-Hassan, Hayat, R., Nasim, W., Akmal, M., Mubeen, M., Hussain, S., & Ahmad, S. (2021). Nutrient Dynamics and the Role of Modeling. In W. N. Jatoi, M. Mubeen, A. Ahmad, M. A. Cheema, Z. Lin, & M. Z. Hashmi (Eds.), *Building Climate Resilience in Agriculture: Theory, Practice and Future Perspective* (pp. 297–316). Springer International Publishing. https://doi.org/10.1007/978-3-030-79408-8_19

Ahrens, A., Llewellyn, D., & Zheng, Y. (2023). Is Twelve Hours Really the Optimum Photoperiod for Promoting Flowering in Indoor-Grown Cultivars of Cannabis sativa? *Plants*, *12*(14), 2605. https://doi.org/10.3390/plants12142605

Altland, J. E. (2021). The Pour-Through Procedure for Monitoring Container Substrate Chemical Properties: A Review. *Horticulturae*, *7*(12), 536. https://doi.org/10.3390/horticulturae7120536

Balboa, G. R., Sadras, V. O., & Ciampitti, I. A. (2018). Shifts in Soybean Yield, Nutrient Uptake, and Nutrient Stoichiometry: A Historical Synthesis-Analysis. *Crop Science*, *58*(1), 43–54. https://doi.org/10.2135/cropsci2017.06.0349

Barrow, N. J., Asif, Sk. Md., & Debnath, A. (2024). Reaction of Organic Phosphates with Oxides: Effects on pH, the Equation Used to Describe the Reaction, and on Desorption. *European Journal of Soil Science*, *75*(1), e13462. https://doi.org/10.1111/ejss.13462

Bauerle, W. L., McCullough, C., Iversen, M., & Hazlett, M. (2020). Leaf Age and Position Effects on Quantum Yield and Photosynthetic Capacity in Hemp Crowns. *Plants*, *9*(2), 271. https://doi.org/10.3390/plants9020271

Baumgardner, J. L., Bauerle, W. L., & Eilertson, K. (2021). Estimating Optimal Daily Nitrate, Potassium, and Water Requirements of *Cannabis Sativa* 'Cherry Wine' During the Vegetative Phase. *Journal of Plant Nutrition*, 1–11. https://doi.org/10.1080/01904167.2020.1867741

Bender, R. R., Haegele, J. W., & Below, F. E. (2015). Nutrient Uptake, Partitioning, and Remobilization in Modern Soybean Varieties. *Agronomy Journal*, *107*(2), 563–573. https://doi.org/10.2134/agronj14.0435

Bernstein, N., Gorelick, J., Zerahia, R., & Koch, S. (2019). Impact of N, P, K, and Humic Acid Supplementation on the Chemical Profile of Medical Cannabis (*Cannabis sativa* L.). *Frontiers in Plant Science*, *10*, 736. https://doi.org/10.3389/fpls.2019.00736

Bevan, L., Jones, M., & Zheng, Y. (2021). Optimisation of Nitrogen, Phosphorus, and Potassium for Soilless Production of *Cannabis sativa* in the Flowering Stage Using Response Surface Analysis. *Frontiers in Plant Science*, *12*, 764103. https://doi.org/10.3389/fpls.2021.764103

Blok, C., Voogt, W., & Barbagli, T. (2023). Reducing nutrient imbalance in recirculating drainage solution of stone wool grown tomato. *Agricultural Water Management*, *285*, 108360. https://doi.org/10.1016/j.agwat.2023.108360

Bugbee, B. (2004). Nutrient Management in Recirculating Hydroponic Culture. *Acta Horticulturae*, (648), 99–112. https://doi.org/10.17660/ActaHortic.2004.648.12

Caplan, D., Stemeroff, J., Dixon, M., & Zheng, Y. (2018). Vegetative Propagation of Cannabis by Stem Cuttings: Effects of Leaf Number, Cutting Position, Rooting Hormone, and Leaf Tip Removal. *Canadian Journal of Plant Science*, *98*(5), 1126–1132. https://doi.org/10.1139/cjps-2018-0038

Cedeño, J., Magán, J. J., Thompson, R. B., Fernández, M. D., & Gallardo, M. (2023). Reducing Nutrient Loss in Drainage from Tomato Grown in Free-Draining Substrate in Greenhouses Using Dynamic Nutrient Management. *Agricultural Water Management*, *287*, 108418. https://doi.org/10.1016/j.agwat.2023.108418

Cedeño, J., Magán, J.-J., Thompson, R. B., Fernández, M.-D., & Gallardo, M. (2024). Comparison of Methods to Determine Nutrient Uptake of Tomato Grown in Free-Draining Perlite Substrate—Key Information for Optimal Fertigation Management. *Horticulturae*, *10*(3), Article 3. https://doi.org/10.3390/horticulturae10030232

Chen, Q., Shinozaki, D., Luo, J., Pottier, M., Havé, M., Marmagne, A., Reisdorf-Cren, M., Chardon, F., Thomine, S., Yoshimoto, K., & Masclaux-Daubresse, C. (2019). Autophagy and Nutrients Management in Plants. *Cells*, *8*(11), 1426. https://doi.org/10.3390/cells8111426

Cockson, P., Schroeder-Moreno, M., Veazie, P., Barajas, G., Logan, D., Davis, M., & Whipker, B. E. (2020). Impact of Phosphorus on Cannabis sativa Reproduction, Cannabinoids, and Terpenes. *Applied Sciences*, *10*(21), 7875. https://doi.org/10.3390/app10217875

Cogley, J. G. (2010). Mass-Balance Terms Revisited. *Journal of Glaciology*, *56*(200), 997–1001. https://doi.org/10.3189/002214311796406040

Cui, X. (2012). Nutrient Sensing in Plants. *Molecular Plant*, *5*(6), 1167–1169. https://doi.org/10.1093/mp/sss107

Fathidarehnijeh, E., Nadeem, M., Cheema, M., Thomas, R., Krishnapillai, M., & Galagedara, L. (2023). Current Perspective on Nutrient Solution Management Strategies to Improve the Nutrient and Water Use Efficiency in Hydroponic Systems. *Canadian Journal of Plant Science*, *104*(2), 88–102. https://doi.org/10.1139/cjps-2023-0034

Fuentes-Peñailillo, F., Gutter, K., Vega, R., & Silva, G. C. (2024). New Generation Sustainable Technologies for Soilless Vegetable Production. *Horticulturae*, *10*(1), 49. https://doi.org/10.3390/horticulturae10010049

Griffiths, M., & York, L. M. (2020). Targeting Root Ion Uptake Kinetics to Increase Plant Productivity and Nutrient Use Efficiency. *Plant Physiology*, *182*(4), 1854–1868. https://doi.org/10.1104/pp.19.01496

Hawkesford, M. J., Horst, W., Kichey, T., Lambers, H., Schjoerring, J., Skrumsager Moller, I., & White, P. (2012). *Functions of macronutrients* (P. Marschner, Ed.; pp. 135–189). Academic Press Amsterdam, Netherlands. https://doi.org/10.1016/B978-0-12-384905-2.00006-6

He, M., Zhang, K., Tan, H., Hu, R., Su, J., Wang, J., Huang, L., Zhang, Y., & Li, X. (2015). Nutrient Levels Within Leaves, Stems, and Roots of the Xeric Species Reaumuria Soongorica in Relation to Geographical, Climatic, and Soil Conditions. *Ecology and Evolution*, *5*(7), 1494–1503. https://doi.org/10.1002/ece3.1441

Hershkowitz, J. A., Westmoreland, F. M., & Bugbee, B. (2025). Elevated Root-Zone P and Nutrient Concentration Do Not Increase Yield or Cannabinoids in Medical Cannabis. *Frontiers in Plant Science*, *16*, 1433985. https://doi.org/10.3389/fpls.2025.1433985

Hinsinger, P. (2001). Bioavailability of Soil Inorganic P in the Rhizosphere as Affected by Root-Induced Chemical Changes: A Review. *Plant and Soil*, *237*(2), 173–195. https://doi.org/10.1023/A:1013351617532

Houston, L. (2021). *Nutrient Uptake and Management Strategies in Recirculating Hydroponic Systems* [Master's thesis, University of Arkansas]. https://scholarworks.uark.edu/etd/4279

Ingestad, T. (1982). Relative Addition Rate and External Concentration; Driving Variables Used in Plant Nutrition Research. *Plant, Cell & Environment*, *5*(6), 443–453. https://doi.org/10.1111/1365-3040.ep11611714

Jiang, D., Gong, H., Niklas, K. J., & Wang, Z. (2024). Allocation of Nitrogen and Phosphorus in the Leaves, Stems, and Roots of Artemisia: A Case Study in Phylogenetic Control. *Frontiers in Plant Science*, *15*, 1445831. https://doi.org/10.3389/fpls.2024.1445831

Jing, G., Hu, T., Liu, J., Cheng, J., & Li, W. (2020). Biomass Estimation, Nutrient Accumulation, and Stoichiometric Characteristics of Dominant Tree Species in the Semi-Arid Region on the Loess Plateau of China. *Sustainability*, *12*(1), 339. https://doi.org/10.3390/su12010339

Juarez-Maldonado, A., Alba-Romenus, K., Morales-Diaz, A. B., & Benavides-Mondoza, A. (2017). Macro-nutrient uptake dynamics in greenhouse tomato crop. *Journal of Plant Nutrition*, *40*(13), 1864–1876.

Konvalina, P., Neumann, J., Hoang, T. N., Bernas, J., Trojan, V., Kuchař, M., Lošák, T., & Varga, L. (2024). Effect of Light Intensity and Two Different Nutrient Solutions on the Yield of Flowers and Cannabinoids in *Cannabis sativa* L. Grown in Controlled Environment. *Agronomy*, *14*(12), 2960. https://doi.org/10.3390/agronomy14122960

Landis, H., Hicks, K., Cockson, P., Henry, J. B., Smith, J. T., & Whipker, B. E. (2019). Expanding Leaf Tissue Nutrient Survey Ranges for Greenhouse Cannabidiol-Hemp. *Crop, Forage & Turfgrass Management*, *5*(1), 180081. https://doi.org/10.2134/cftm2018.09.0081

Langenfeld, N. J., & Bugbee, B. (2024). Sustainable Hydroponics Using Zero-discharge Nutrient Management and Automated pH Control. *HortScience*, *59*(8), 1202–1206. https://doi.org/10.21273/HORTSCI17975-24

Langenfeld, N. J., Pinto, D. F., Faust, J. E., Heins, R., & Bugbee, B. (2022). Principles of Nutrient and Water Management for Indoor Agriculture. *Sustainability*, *14*(16), 10204. https://doi.org/10.3390/su141610204

Li, Y., Zhang, S., Guo, W., Zheng, W., Zhao, Q., Yu, W., & Li, J. (2024). Effects of irrigation scheduling on the yield and irrigation water productivity of cucumber in coconut coir culture. *Scientific Reports*, *14*(1), 2944. https://doi.org/10.1038/s41598-024-52972-x

Marschner, H. (2012). *Marschner's Mineral Nutrition of Higher Plants* (3rd ed.). Academic Press.

Massuela, D. C., Munz, S., Hartung, J., Nkebiwe, P. M., & Graeff-Hönninger, S. (2023). Cannabis Hunger Games: Nutrient Stress Induction in Flowering Stage – Impact of Organic and Mineral Fertilizer Levels on Biomass, Cannabidiol (CBD) Yield and Nutrient Use Efficiency. *Frontiers in Plant Science*, *14*, 1233232. https://doi.org/10.3389/fpls.2023.1233232

MathWorks. (n.d.). *ThingSpeak channels*. MathWorks. Retrieved October 27, 2025, from https://thingspeak.mathworks.com/channels

National Oceanic and Atmospheric Administration. (n.d.). *Solar calculator*. NOAA Global Monitoring Laboratory. Retrieved October 27, 2025, from https://gml.noaa.gov/grad/solcalc/

Ontario Ministry of the Environment, Conservation and Parks (MECP). (2022). *O. Reg. 300/14: Greenhouse nutrient feedwater (under the Nutrient Management Act, 2002, S.O. 2002, c. 4)*. Queen's Printer for Onterio. https://www.ontario.ca/laws/regulation/140300

Parent, S. E., Parent, L. E., Rozanne, D. E., Hernandes, A., & Natale, W. (2012). Nutrient Balance as Paradigm of Soil and Plant Chemometrics. In R. Issaka (Ed.), *Soil Fertility*. InTech. https://doi.org/10.5772/53343

Powell, K., & Bauerle, W. L. (2026). Predicting vegetative phase nutrient uptake in Cannabis sativa L. via transpiration-driven mass-balance. *Frontiers in Plant Science*, *16*, 1753553. https://doi.org/10.3389/fpls.2025.1753553

R Foundation for Statistical Computing. (2024). *R Core Team. R: A language and environment for statistical computing.* (Version 4.3.1) [Computer software]. www.R-project.org

Ram, H., Gandass, N., Sharma, A., Singh, A., Sonah, H., & Deshmukh, R. (2020). Spatio-Temporal Distribution of Micronutrients in Rice Grains and Its Regulation. *Biotechnology*, *40*(4). https://www.tandfonline.com/doi/abs/10.1080/07388551.2020.1742647

Saloner, A., & Bernstein, N. (2020). Response of Medical Cannabis (*Cannabis sativa* L.) to Nitrogen Supply Under Long Photoperiod. *Frontiers in Plant Science*, *11*, 572293. https://doi.org/10.3389/fpls.2020.572293

Saloner, A., & Bernstein, N. (2021). Nitrogen supply affects cannabinoid and terpenoid profile in medical cannabis (*Cannabis sativa* L.). *Industrial Crops and Products*, *167*, 113516. https://doi.org/10.1016/j.indcrop.2021.113516

Saloner, A., & Bernstein, N. (2022). Effect of Potassium (K) Supply on Cannabinoids, Terpenoids and Plant Function in Medical Cannabis. *Agronomy*, *12*(5), 1242. https://doi.org/10.3390/agronomy12051242

Saloner, A., & Bernstein, N. (2023). Dynamics of Mineral Uptake and Plant Function during Development of Drug-Type Medical Cannabis Plants. *Agronomy*, *13*(12), 2865. https://doi.org/10.3390/agronomy13122865

Saloner, A., Sacks, M. M., & Bernstein, N. (2019). Response of Medical Cannabis (*Cannabis sativa* L.) Genotypes to K Supply Under Long Photoperiod. *Frontiers in Plant Science*, *10*, 1369. https://doi.org/10.3389/fpls.2019.01369

Shen, J., Yuan, L., Zhang, J., Li, H., Bai, Z., Chen, X., Zhang, W., & Zhang, F. (2011). Phosphorus Dynamics: From Soil to Plant1. *Plant Physiology*, *156*(3), 997–1005. https://doi.org/10.1104/pp.111.175232

Shiponi, S., & Bernstein, N. (2021). Response of Medical Cannabis (*Cannabis Sativa* L.) Genotypes to P Supply Under Long Photoperiod: Functional Phenotyping and the Ionome. *Industrial Crops and Products*, *161*, 113154. https://doi.org/10.1016/j.indcrop.2020.113154

Silber, A., Naor, A., Cohen, H., Bar-Noy, Y., Yechieli, N., Levi, M., Noy, M., Peres, M., Duari, D., Narkis, K., & Assouline, S. (2018). Avocado fertilization: Matching the periodic demand for nutrients. *Scientia Horticulturae*, *241*, 231–240. https://doi.org/10.1016/j.scienta.2018.06.094

Silberbush, M., & Ben-Asher, J. (2001). Simulation Study of Nutrient Uptake by Plants from Soilless Cultures as Affected by Salinity Buildup and Transpiration. *Plant and Soil*, *233*(1), 59–69.

Sonneveld, C., & Voogt, W. (2009). Plant Nutrition in Future Greenhouse Production. In C. Sonneveld & W. Voogt (Eds.), *Plant Nutrition of Greenhouse Crops* (pp. 393–403). Springer Netherlands. https://doi.org/10.1007/978-90-481-2532-6_17

Sperling, O. (2020). (PDF) Precise Fertilization by a Mass-Balance of the Seasonal Changes in Nutrient Uptake by Almond Trees. *ResearchGate*. https://doi.org/10.3390/agronomy10091277

Sperling, O., Karunakaran, R., & Yermiyahu, U. (2020). Precise Fertilization by a Mass-Balance of the Seasonal Changes in Nutrient Uptake by Almond Trees. *Agronomy*, *10*(9), 1277. https://doi.org/10.3390/agronomy10091277

Sulaiman, H., Yusof, A. A., & Mohamed Nor, M. K. (2025). Automated Hydroponic Nutrient Dosing System: A Scoping Review of pH and Electrical Conductivity Dosing Frameworks. *AgriEngineering*, *7*(2), 43. https://doi.org/10.3390/agriengineering7020043

Tang, K., Fracasso, A., Struik, P. C., Yin, X., & Amaducci, S. (2018). Water and Nitrogen Use Efficiencies of Hemp (*Cannabis sativa* L.) Based on Whole-Canopy Measurements and Modeling. *Frontiers in Plant Science*, *9*, 951. https://doi.org/10.3389/fpls.2018.00951

Velechovský, J., Malík, M., Šenkyřík, J. B., & Tlustoš, P. (2024). Effect of Augmented Nutrient Composition and Fertigation System on Biomass Yield and Cannabinoid Content of Medicinal Cannabis (*Cannabis Sativa* L.) Cultivation. *Frontiers in Plant Science*, *15*. https://doi.org/10.3389/fpls.2024.1322824

Westmoreland, F. M., & Bugbee, B. (2022). Sustainable Cannabis Nutrition: Elevated Root-Zone Phosphorus Significantly Increases Leachate P and Does Not Improve Yield or

Quality. *Frontiers in Plant Science*, *13*, 1015652. https://doi.org/10.3389/fpls.2022.1015652

White, P. J., & Broadley, M. R. (2003). Calcium in plants. *Annals of Botany*, *92*(4), 487–511.

White, P. J., & Brown, P. H. (2010). Plant nutrition for sustainable development and global health. *Annals of Botany*, *105*(7), 1073–1080. https://doi.org/10.1093/aob/mcq085

Xu, G., Fan, X., & Miller, A. J. (2012). Plant Nitrogen Assimilation and Use Efficiency. *Annual Review of Plant Biology*, *63*(Volume 63, 2012), 153–182. https://doi.org/10.1146/annurev-arplant-042811-105532